MINISTERUL EDUCAȚIEI
UNIVERSITATEA TEHNICĂ
DIN CLUJ-NAPOCA

Field Electrical Engineering

PhD THESIS
– ABSTRACT –

Research on the assessment of human exposure to electromagnetic fields generated by communication systems

Phd Student:
Delia-Bianca Deaconescu

PhD Supervisor:
Prof. Dr. Ing. Simona Miclăuș

Examination committee:

Chair: Prof. Eng. **Călin Munteanu,** PhD – Technical University of Cluj-Napoca;
PhD Supervisor: Prof. Eng. **Simona Miclăuș** – PhD – Technical University of Cluj-Napoca;
Members:
- Prof. Eng. **Aldo de Sabata** – PhD Polytechnic University of Timișoara;
- Prof. Dr. Ing. **Răzvan Tamaș** – PhD Maritime University of Constanța;
- Conf. Dr. Ing. **Șerban Obreja** – PhD Polytechnic University of Bucharest.

– Cluj-Napoca –
2024

CONTENTS OF PhD THESIS

INTRODUCTION

The electromagnetic field, along with the gravitational field, represents the two fundamental long-range force fields in nature, and governs the interaction at a distance through electric and magnetic charges. When the electromagnetic field passes through matter, a series of complex physical and chemical interactions take place that depend on the frequency and intensity of the electromagnetic field, as well as the properties of the material. If the crossed material is a living biological one, the effects can be different from the case of non-living dielectric materials. The field of knowledge that studies the interaction of electromagnetic fields with biological structures is called bioelectromagnetics, and in recent decades research in this field has developed rapidly, in line with the increasingly intensive and varied use of technologies that emit electromagnetic waves.

The last two decades have shown an unprecedented development of communication technologies using radio frequency electromagnetic field sources used for individual, industrial, medical and commercial purposes. From global communications and rapid access to information, to industrial automation and the development of smart cities, the use of radio frequencies has revolutionized the way we live and work. Although the exponential proliferation of new communication devices have facilitated and facilitated human activity, they have led to a growing concern about the impact on human health. In this regard, a growing number of researches have focused on the effects of the interaction between electromagnetic fields and living matter, both in the short term and in the long term. Therefore, both the beneficial effects produced as a result of the interaction of the electromagnetic field with living tissues, such as the case of hyperthermia in which microwave energy is used to destroy tumor cells by their local heating, as well as possible adverse effects on health are studied.

In the context of human exposure to electromagnetic fields, exposure and dosimetry are essential methods used to measure and assess radiation exposure, as well as in the development of appropriate protective measures. Exposimetry involves measuring the fields generated by the emitting devices in the air, at the incidence on the human body. Dosimetry consists in measuring and evaluating the dose of radiation actually absorbed by a biological material inside it, quantified with the help of the specific absorption rate (SAR). Since the main effect of the interaction of radiofrequency fields with biological materials is dielectric heating, and due to the impossibility of measuring the level of temperature increase in tissues (invasive action), effective simulation programs have been developed, based on numerical methods for calculating the propagation of electromagnetic waves in biological matter. One such software program, also used in this work, is CST Microwave Studio, which implements Maxwell's equations in integral and differential form and solves them spatio-temporally.

In this PhD thesis, the assessment of human exposure caused by communication systems was analyzed from the perspective of two complementary approaches. The first one refers to the determination of the exposure of the human body to electromagnetic emissions in the near field in the case of using a mobile phone, and the second approach involves the determination of the population's exposure to radio emissions in the far field, emissions coming from the antennas of the base stations in the networks mobile phone.

Along with technological progress, there have also been recommendations provided by accredited international bodies, regarding the maximum permissible values of exposure or absorption of electromagnetic energy in the body. These guidelines and standards are designed to protect human health and ensure that exposure levels remain within protective limits.

The main and most important source of radio frequency waves used near the human body is the mobile phone. The regulations in force provide limits regarding the maximum power radiated by the mobile terminal, but the diversity of existing models and the way they are used by users make it difficult to accurately and specifically quantify the intensity of the incident field, which is why the first previously mentioned approach deepens this type of research. The development of the new generation of 5G mobile communication technologies has raised a multitude of concerns among the general public regarding the amount of energy radiated by such equipment, especially the increase in the frequency used causes the intrinsic increase in the energy emitted. Recently, the prevalence of human exposure due to the mobile phone (in this case for the 4G and 5G generations) and not to the antennas of base stations at height on buildings or towers has been demonstrated. However, the study of the dynamics of signals emitted by a mobile phone is extremely poorly represented in the literature, precisely because until very recently no emphasis was placed on the temporal variability and the values of the crest factors of the emitted signals. However, studying the temporal dynamics of human exposure is complementary and very useful, as it can provide information related to the identification of the causes of non-thermal and athermal effects of radio frequencies. Practically, the focus shifts from the notion of dose to that of dose rate, to that of instantaneous and average rate of accumulation of electromagnetic energy. The electromagnetic exposure of a person while using the mobile terminal for various voice or data applications has remained one of the challenging aspects to be investigated, especially in 4G and 5G mobile communication networks, due to the very high variability of emitted signals in time and space (including by implementing beamforming and beamsteering techniques).

This PhD thesis aims to investigate in detail the amplitude-time-frequency peculiarities of signals emitted by 4G and 5G mobile communication systems, as well as to analyze human exposure to such radiation sources in different exposure scenarios.

The work contains a number of 251 pages, having two distinct parts. In the first part, the fundamental elements are presented, those that refer to the communication standards, respectively to the modulation and coding schemes of the signals - which will have a massive impact on the way of setting the spectrum analyzers used in the experimental precision measurements, as well as to the dielectric characteristics of the tissues and the peculiarities of the biological response to these types of stimuli. The current state of knowledge in the field on the two mentioned levels is presented and the research niches that need to be solved are identified. The second part of the thesis, more voluminous, includes case studies and personal contributions. In total, the thesis is structured on 12 chapters and 5 private studies.

In the first chapter, the evolution of mobile communication systems is presented, starting from technologies that used analog transmissions to those based on digital transmissions. The main characteristics of each generation of communications are described, as well as the need to implement the 5G NR architecture.

Chapter 2 presents the characteristics of signals specific to the 4G LTE communications standard. Concepts of frequency spectrum allocation, the basic technologies used by the 4G standard and network architecture are presented.

Chapter 3 highlights the technical specifications of the new generation of 5G mobile communications implemented starting in 2020 in Romania. For a comparative analysis with the already existing generations of communications, in this chapter were presented: the mode of frequency spectrum allocation, the structure of the NR data frame, the network architecture and the dynamic spectrum allocation in the two 4G and 5G standards. Beamforming and beamsteering techniques were also described in detail, which constitute the essential foundations that underpinned the development of 5G technology.

The 4th chapter includes general notions about electromagnetic waves, the main electromagnetic field sources being reviewed. In order to understand the phenomena of interaction of the electromagnetic field with living matter, the dielectric characteristics of biological environments, notions of dosimetry and the connection between external fields and those induced inside biological structures were presented. A synthesis of the current state of biological effects and on the human body was also made.

Chapter 5 first presents the main rules and regulations for the protection of human health against exposure to electromagnetic field sources. Emphasis was placed on the norms recommended by ICNIRP, as they are adopted in most European countries. In the framework of the thesis, the values obtained from the experimental studies for the electromagnetic field level were reported to the limits established by ICNIRP. In the last part of the chapter, we analyzed the peculiarities of the wave propagation simulation environment, CST MWS, used in the application part in order to evaluate by simulation the human exposure to emission sources that use beamforming and beamsteering techniques.

In the 6th chapter, the general and particular objectives of the research carried out during the doctoral internship are presented.

In chapter 7, the data collected from 7 fixed sensors from the national electromagnetic monitoring network of the National Authority for Administration and Regulation in Communications (ANCOM) in the city of Bucharest, in areas with intense radio traffic, were pre-processed and processed. The peak and average values, statistical distributions and other processing of the time series of the measured electric field strength were analyzed and interpreted during 13 months.

Chapter 8 addresses the identification of time signatures of emissions from base stations (downlink signals) and mobile phones (uplink signals) specific to the 4G LTE communication standard from the perspective of recurrence analysis.

Chapter 9 highlights the results obtained from the experimental evaluation of the dynamics of the field radiated by a mobile phone connected to 4G and 5G commercial communication networks and highlights the distinctive features.

Chapter 10 quantifies the difference between 4G and 5G signal dynamics using statistical, non-linear, and graphical analysis methods and leverages the utility of a deep learning algorithm based on neural networks in recognizing and classifying cell phone emission types in depending on the application used on the phone.

Chapter 11 presents the results of numerical dosimetry analyzes carried out with the help of the CST MWS simulation environment, which highlight the influence of the use of phased antennas on the spatial distribution of the incident electric field on an anthropomorphic model of a human head and the specific rate of energy absorption in the respective model, from the perspective of the use of beam emissions from 5G.

Chapter 12 captures the final conclusions, the contributions of the doctoral thesis to knowledge in the field as well as future research directions.

In conclusion, this thesis offers a complementary, niche approach to the field of human exposure assessment to electromagnetic radiation emitted by the latest and used generations of radio frequency and microwave sources, as well as the promotion of new modern techniques and methods of time series analysis , of the variability of the signals, the recurrence and the stochastic or deterministic nature of the emissions.

Objectives and research directions

The research approach in this phd thesis is structured around five comprehensive studies, each of which was carried out in order to explore and develop the fields of

experimental exposure and radiofrequency dosimetry. The general objective is to determine the level of human exposure to electromagnetic radiation emitted by communication systems in different scenarios, simultaneously with the time-frequency-amplitude analysis of the signals emitted by the investigated sources. The research aims at the applicability of different methods of accurate quantification of the intensity level of the electric field of radio frequency and microwaves corroborated with methods used in other fields (e.g. medical, economic, etc.) in the analysis of the spatio-temporal variability of the emitted waves.

The main directions of research consist of:

1) *Evaluation of human exposure to electromagnetic fields in urban areas: the city of Bucharest. This direction includes the following objectives*:

   a) Processing the data of field intensities measured by the fixed radio monitoring stations in the ANCOM national network, in order to identify the population exposure percentage in relation to the reference levels established by the regulations in force and to express the temporal dynamics in the short and medium term;
   b) The use of descriptive statistical methods in order to identify the amplitude-time-frequency characteristics of signals captured in broadband and in narrow spectral bands, corresponding to downlink emissions in 2G, 3G and 4G networks.

2) *Comparison of exposure levels to electromagnetic radiation from cellular network base station antennas and mobile phones. This direction includes the following objectives:*

   a) Determination of the power level of emissions generated by base stations connected to commercial networks in the 4G mobile communications standard;
   b) Experimental determination of the power level of the emissions generated by a mobile phone connected to the 4G cellular communications network;
   c) Determining the predictable, deterministic or random character of the emitted field levels, with the help of recurrence analysis. The quantification of the recurrence will provide the possibility to perform the prediction of the temporal profile of the exposure.

3) *Analysis of the evolution of the dynamics of signals emitted by mobile terminals connected to commercial communications networks in 4G and 5G standards. This direction includes the following objectives:*

   a) Analysis of the temporal characteristics of 4G and 5G signals and risk estimation from the perspective of specific effects due to high emission crest factors and specific amplitude distributions. This study will provide a comparative assessment of the exposure profile to the two generations of emission technologies, providing a complementary estimate of the evolution of the dose rate absorbed by the impacted biological environments;

b) Determining the time stamp of mobile phone usage as a result of running five different types of mobile applications. This objective contributes to the evaluation of the intensity level of the electric field recorded for each type of application run on the phone, also providing a vision of the quality of service according to the network to which the mobile terminal is connected;
c) The use of an image (spectrogram) detection and classification algorithm based on a convolutional neural network in order to recognize and classify radio emissions while running mobile applications on the phone. Checking the accuracy of detection and classification of the type of mobile application that emits the signals constitutes the basis for the further development of an integrated system for exposure profiling.

4) Investigating the influence of communication system infrastructure design and 5G communication network architecture on the spatial distribution of tissue absorbed radiation. This direction includes the following objectives:

a) Implementation, testing and evaluation of beamforming and beamsteering performances in the design of 5G generation smart antennas. This aspect helps to determine the optimal parameters of adaptive antennas;
b) Identification of exposure scenarios related to minimizing human exposure without compromising antenna performance;
c) Determination of the values of the specific rate of absorption and radio energy in tissues and the intensity level of the incident electric field for different scenarios of exposure of an anthropomorphic model of a human head to the radiation emitted by adaptive antennas.

PERSONAL CONTRIBUTION

Study 1 - Evaluation of the level of the radio frequency field in urban areas - the case of the city of Bucharest, using the data recorded by the fixed network of monitoring sensors of ANCOM

Materials and methods

The fixed monitoring sensors installed by ANCOM in the localities on the territory of Romania use a triaxial isotropic antenna for measuring the intensity of the electric field in four different frequency bands:
a broadband that includes the frequency range 100 kHz – 7GHz – this band also includes the bands used in Romania for 5G-FR1 mobile communications;

- three frequency bands in the 2G-4G mobile spectrum: 925 – 960 MHz (GSM900), 1805 – 1880 MHz (GSM 1800) and 2110 – 2170 MHz (UMTS).

The monitoring system is composed of measuring stations equipped with NARDA AMB 8057 or AMB 8059 type sensors that monitor the electromagnetic field permanently. These sensors cover a wide range of frequencies (9 kHz – 7 GHz) and measure electromagnetic field strengths from a few tenths of μV/m to hundreds of V/m. The sensors are designed to withstand complex environments, including extreme weather conditions, making them ideal for long-term outdoor use. Fixed sensors use broadband measurement technology to simultaneously cover all frequencies within a specified range without requiring frequent adjustments. For the analysis and interpretation of the recorded data, the sensors are compatible with the Narda software program.

At the level of the municipality of Bucharest, currently, in the year 2024, there are 15 fixed monitoring stations.

In the present study, we chose to analyze and interpret data from 7 fixed sensors that are installed in the most populated areas of the city.

In this research, the data recorded by the seven monitoring stations in the city of Bucharest, over a period of 13 months, between 01.09.2022 and 30.09.2023, were analyzed. Later, a comparative analysis of the electromagnetic field levels recorded in the months of January, February and March related to the years 2023 and 2024 was carried out. In this sense, the analyzed database totaled over 2 million samples.

Results and discussions

Figure 1 shows boxplot graphs that highlight the mean, median and interquartile range (IQR) for the electric field intensity (peak values and average values) measured during 13 months in the four frequency bands, in the seven locations in the municipality Bucharest. For the frequency range 100 kHz – 7 GHz in the case of station 7 we observe the largest IQR intervals in which the electric field values are scattered. Also, from the point of view of exposure in this case, the highest values of Eavg (13.34 V/m) and Epeak (38.67 V/m) were determined. The lowest values of the electric field intensity were recorded at the North Station location (Station 5). We highlight an intensified presence of outliers marked by diamonds of the electric field intensity in the cases of Epeak (S2), Eavg (S3), Epeak (S3), Epeak (S5) and Eavg (S5). In this situation the outliers show significantly higher values than the

other data centered in the IQR interval. Also these outliers together with the asymmetry of the box and whiskers indicate a high variability and a non-uniform distribution of the electric field values. In broadband, the average of the electric field intensity values is approximately double compared to their average in the three frequency bands specific to mobile communications. This behavior reveals the presence of a larger number of emission devices in use, as well as the use of new equipment configured in the 5G communication network.

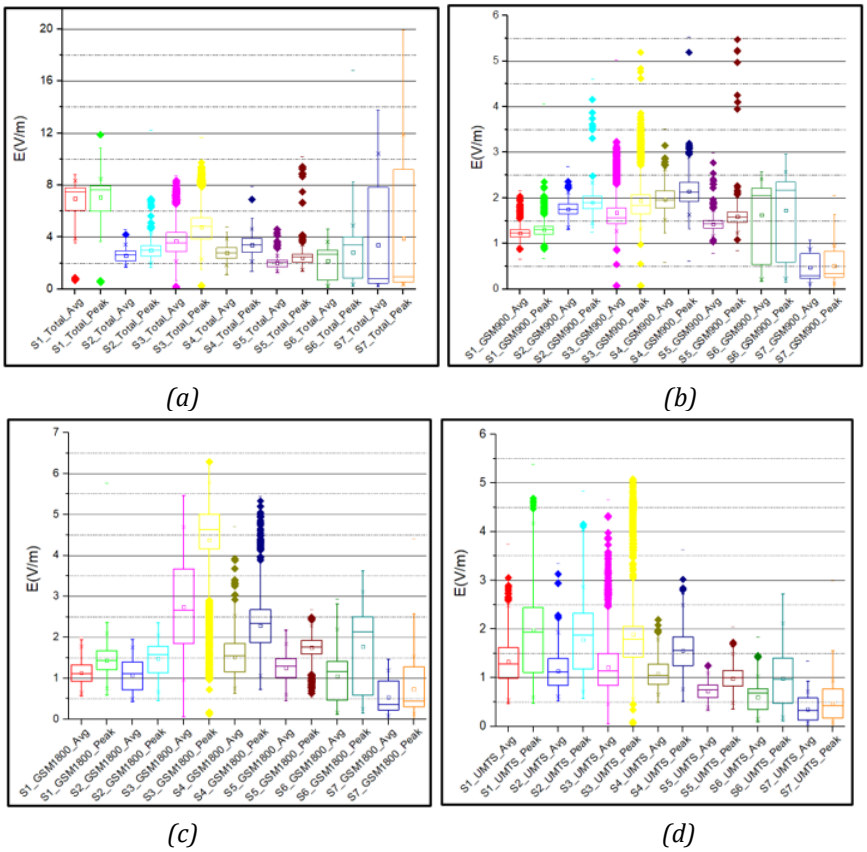

Figure 1 Boxplot representations of the average and peak values related to the electric field intensity recorded in the period September 2022 – September 2023: (a) broadband; (b) – (d) selective bands

Figure 2 shows the temporal evolution of the average values of the electric field intensity in the four frequency bands, for 13 months in the seven locations in Bucharest. In the case of the wide frequency band, we note that the highest average values were recorded by stations S1 and S3 for the entire evaluated period, except for the particular case of the values recorded between April and September 2023 by station S7.

From the graphical representations we observed a similar particular case for the values recorded by stations S6 and S7, namely a sudden increase in the level of radiation in fixed time intervals. Therefore, in the case of the field values measured by the S6 station, in all four frequency bands, starting from December 2022 and until July 2023, we observe an increase in its level approximately three times (in the case of the UMTS band) compared to the other periods of time. In the case of the S7 station, a high level of electric field intensity was recorded in the period from April to September 2023 for all frequency bands analyzed.

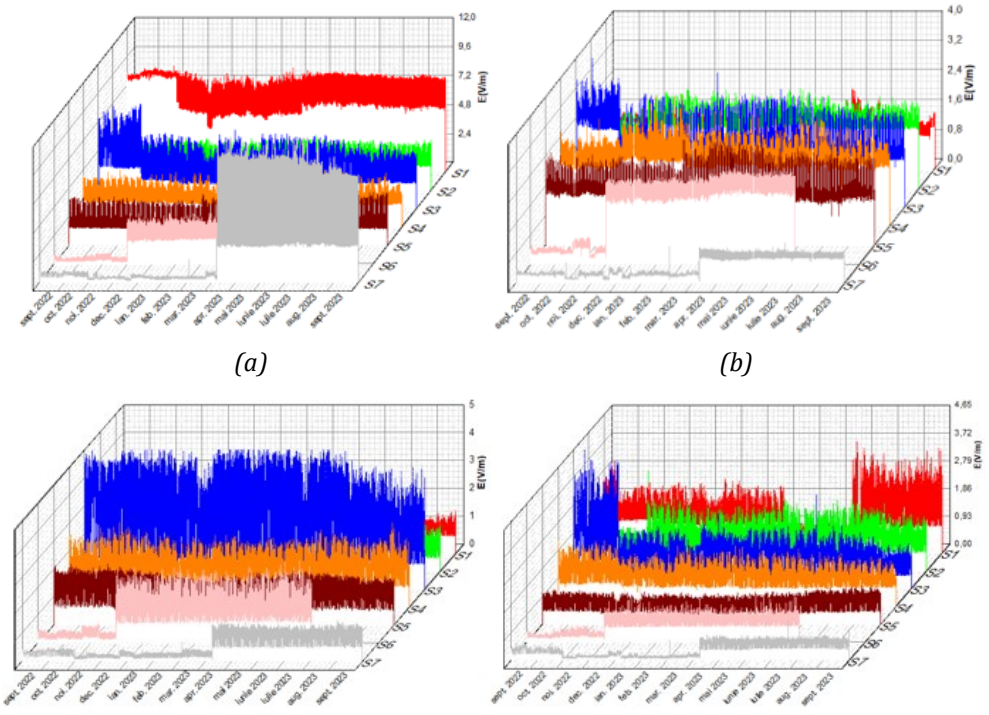

(a) *(b)*

(c) *(d)*

Figure 2 Time variation of Eavg(V/m) measured by the seven stations during September 2022 – September 2023: (a) broadband; (b) GSM900; (c) GSM1800; (d) UMTS

Conclusions

a) in the Hrisovului 24 location, the highest values of the electric field intensity were recorded, as well as the highest variation of the signals in the wide frequency band;

b) the outliers together with the asymmetry of the box and whiskers indicate a high variability and a non-uniform distribution of the electric field values for stations S3 and S5;

c) in broadband, the average of the electric field intensity values is approximately double compared to their average in the three frequency bands specific to mobile communications, behavior also associated with the implementation of the new 5G mobile communications systems.

d) lower short-term exposure variability than long-term variability was present in all situations;

e) a greater variability of the exposure was proven by the majority of points spread outside the entropy, behavior correlated with the presence of outliers revealed by the boxplot diagrams;

f) in the case of stations S6 and S7, the narrow and long shape of the ellipse indicated a correlation between the consecutive values of the signal, the signal presenting a short-term deterministic behavior.

Study 2 – Evaluation of the time signature of emissions from base stations (downlink signals) and mobile phones (uplink signals) specific to the 4G LTE communication standard from the perspective of recurrence analysis

Materials and methods

In order to measure and record the level of power emitted by the cell (uplink emissions), the following instruments were used: a Motorola G 5G plus mobile phone, three spectrum analyzers in real time – from Aaronia model Spectran HF 80120 V5-X and three miniature electric field probes PSB E1.

The following instruments were used to measure and record emissions from LTE base stations: TSMA6 network scanner from Rhode & Schwarz to which were connected: a Qualipoc Android mobile phone and an OmniLOG 90200 antenna from Aaronia, placed on a wooden tripod at a height of 1.5 m from the ground surface.

Results and discussions

In the first stage of the study, we analyzed the recurrence graphs obtained for the data processed in the case of uplink and downlink emissions.

Given the fact that the distribution of colors in the recurrence graphs related to downlink emissions forms certain patterns, for each case of emission, the analyzed signals present a degree of determinism and are structured, not being random.

In the case of uplink emissions, for the file download application, in the case of the three repetitions there are vertical lines, horizontal lines and clusters indicating laminar system states and the fact that the system states are changing slowly. An interesting aspect can be identified in the graphic representation of the recurrences specific to the file upload application, as they are structured and complex (figure 3). In the case of the three repetitions we observe sets of parallel lines (of the same color) with the line of identity (LOI), of different lengths, which indicates the predictability of the signal. The diagonal lines parallel to the LOI represent the parallel trajectories (mirror segments) for the same time evolution.

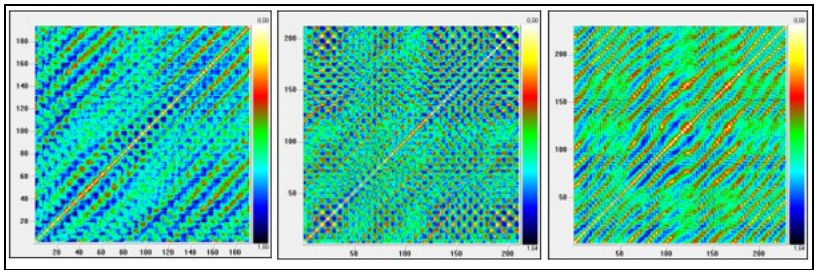

(a) *(b)* *(c)*

Figure 3 Recurrence graphs for file upload - uplink application for: a) R1, b) R2 and c) R3

After analyzing the specific recurrence graphs of the downlink and uplink signals, we noticed that a larger set of data taken by the measurement system provides better clarity on the interpretation of the state of the signals. In the case of downlink signals, several patterns were identified in the graphical representations, which may lead to a connection with the predictability of the time series. In the case of uplink signals, the recurrence graphs show

isolated points as well as white bands indicating non-stationary signals, except for the upload application where the graphs indicate a predictability of the signals.

The recurrence histogram usually shows the characteristic periodicity of the time series. In the case of downlink signals, for day 1 P, Q, R, S emissions we observe similar graphs of the percentage of recurrence, which indicates to us the presence of a degree of recurrence for these data downloads, which decreases as the time gap increases. We also observed a similar behavior for the R and T emissions on day 3. Compared to the recurrence histograms of the downlink signals, the uplink signals show a lower degree of recurrence and a much higher variation. We also see a dense graph structure for the video call, voice and file download apps.

Conclusions

Given the fact that recurrence graphs are structured and form certain patterns, we can affirm the presence of a degree of determinism and the existence of predictable amplitude values.

For the uplink emissions, when using the file downloader we identified behaviors similar to the previous ones, as evaluation of the temporal dynamics indicated slowly changing laminar states. In the case of the mobile streaming application, we noticed non-stationary emissions that showed a certain trend. The graphs of the file upload mobile application indicated a predictability of the signal level because they include lines parallel to the line of identity, which represent the parallel trajectories (mirror segments) for the same evolution over time.

From the recurrence quantification analysis, we found higher values of the determinism parameter in the case of downlink emissions compared to those obtained for uplink signals, an aspect that implies the existence of a deterministic system, more precisely of sequences that repeat at different time intervals .

Study 3 – Determination of the characteristics and dynamics of the emitted field near mobile terminals connected to 4G and 5G commercial communications networks

Materials and methods

In the present experimental study we evaluated the time variation of the electric field strength (E) near a mobile phone connected successively to:

- the 4G LTE network using a channel bandwidth of BW1 = 20 MHz at the center frequency of 2.59 GHz and time division duplexing;
- the 5G NR FR1 network in the n78 band, using a channel bandwidth of BW2 = 40 MHz, at the central frequency of 3.7 GHz and time division duplexing, both networks belonging to the mobile operator RCS&RDS (Digi).

In order to measure and record the power level of the signals emitted by the mobile phone, the following measuring instruments were used: three real-time spectrum analyzers – Spectran 5 (Aaronia) model HF 80120 V5 X and three electric field probes PSB E1 which were positioned at an equal distance from each other and at a distance of 10 cm from the surface of the mobile phone (figure 9.3). A Moto G 5G plus model smartphone (XT 2075-3) with an

emission power of 23 dBm in both 4G and 5G bands was used to evaluate the intensity of the electromagnetic field.

A sampling rate of 100 ms was used for spectrum and data transfer recordings. For each application used, measurements were made in three repetitions (referred to as R1, R2, R3), and each data recording lasted 25 seconds. In the case of measurements made in the 4G network, a real-time bandwidth of 88 MHz was used for the spectrum analyzer, and a real-time bandwidth of 44 MHz was used for the 5G network.

Figure 3 shows the steps related to the algorithm followed in order to measure the emitted power levels in the case of successive use of the two mobile communication networks.

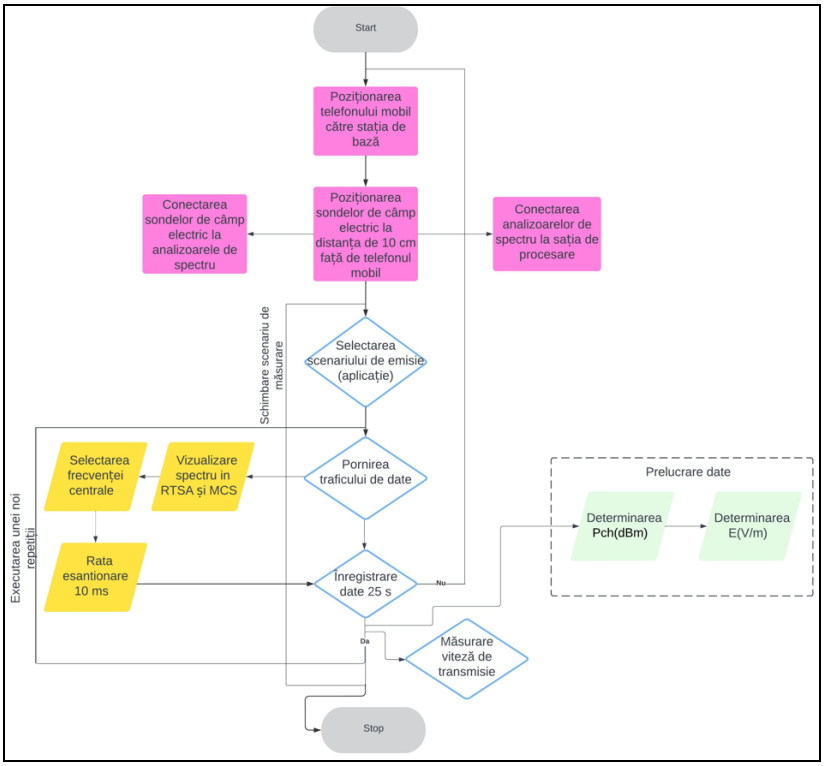

Figure 4 Sequencing of uplink signal level measurement steps

Results and discussions

Figure 5 exemplifies the case of the variation of the electric field intensity in the channel for 25 s, for probe 1, repetition 1. In this sense, we note the maximum value of the electric field intensity of 0.014 V/m, obtained in the case of the 4G standard in the video call application . For the 5G network, the maximum value of the electric field strength (0.012 V/m) was obtained in the case of the streaming application. Carrying out a comparative analysis between the two standards, we notice that the highest electric field values were recorded for the 4G network.

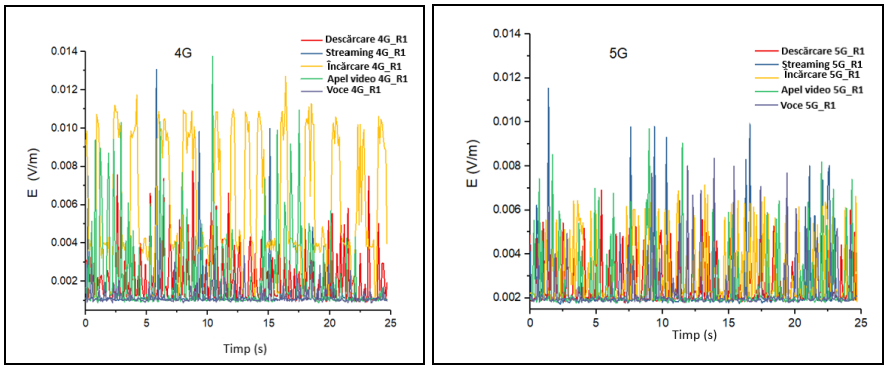

a) *b)*

Figure 5 Time variation of the electric field in the channel measured with probe 1, for the five applications run in: a) the 4G network; b) the 5G network

To observe the differences between the mean slopes, we plotted the graphs in Figure 6 (a). Here, comparing the two communication standards, we can see the average of the accumulated power density rate in the air (in W/m2/s), for each mobile application. We therefore observe several different slopes belonging to 4G applications, and the highest rate of accumulated power density in the air is specific to the file upload application and its value is at least double the other rates. In the case of the 5G standard, the rates are much more similar, but the file upload application still leads to the highest rate of over-the-air accumulation. This integrated approach allowed us, through its metric, to characterize the evolution of electromagnetic exposure over time for the 5G standard, an important technique in addition to the standardized exposure metrics already used in this regard. Next, we calculated the average transmitted power density per bit based on the relationship between the average power density rate and the transfer rate - figure 6 (b). As can be seen, the highest values correspond this time, in both standards, to the streaming application. In all cases, the lowest power density/transmitted bit rates were found in the 5G network.

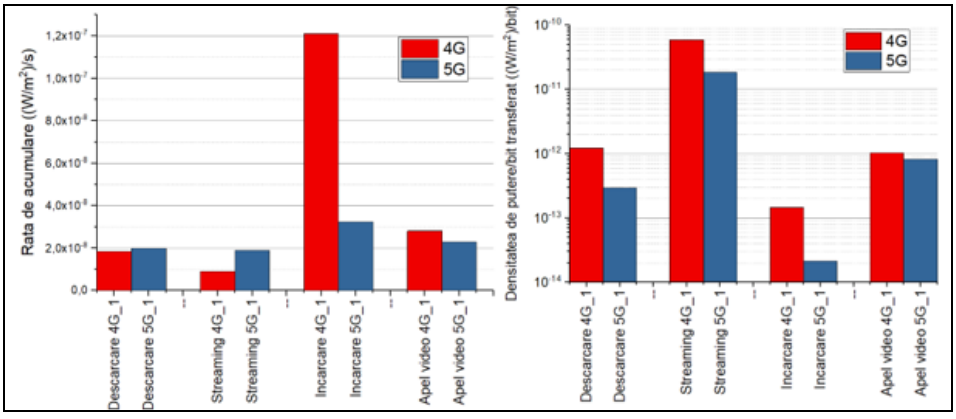

(a) *(b)*

Figure 6 a) Average rate of accumulated incident power density in air for 4G and 5G applications during 25 s; b) Average transmitted power density rate per bit transferred in each situation

The areas of the Poincare ellipse, shown comparatively in figure 7, indicate that the greatest variability of the radiated field corresponds to file upload and video call in 4G. The total variability of emitted fields was higher in the 5G network than in the 4G network for file download, streaming and voice call applications. However, the file upload and video call applications in the 4G standard had at least an order of magnitude more variability than the other applications in both standards. Since this specific feature confirms that file uploading and video calling led to the highest exposure levels in 4G, as inferred from figure 7, it can be

concluded that these applications could be the most interesting for further research in biological dosimetry. In 5G, the largest variations of the radiated field were observed for voice call and file download. These large variabilities may be due to the higher field levels in 5G for these two mobile applications. Therefore, at least voice calls deserve special attention in future dosimetric studies dedicated to the biological effects of 5G signals.

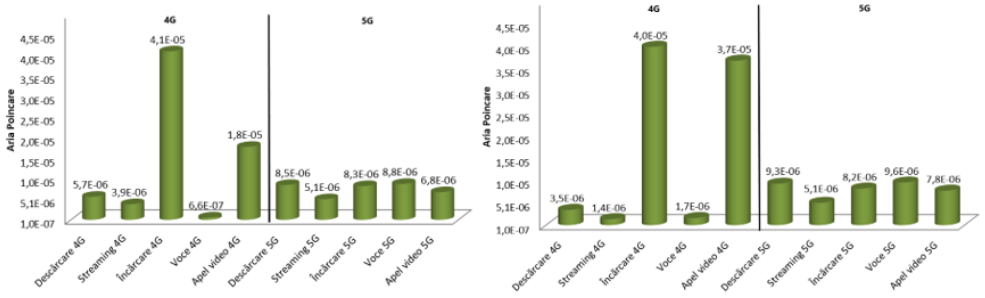

(a) *(b)*

Figure 7 Areas of Poincare maps of electric field strength for all applications in 4G and 5G networks: a) R1; b) R2

Conclusions

Among the most important characteristics identified in this experimental study we list:

- electric field intensities measured in air 10 cm away from the surface of the mobile phone were, on average, 31.7% lower in the 5G network compared to the 4G network, for all verified applications: file upload, file download, streaming, video call and voice call;
- the file uploader provided the highest and most widespread emitted field values in both communication standards;
- the accumulation rate of the power density in the air, at the measurement point, was lower in the 5G standard than in the 4G standard for all applications run, showing greater differences in the case of 4G;
- for all mobile applications, lower values of the average power density emitted per bit of data transferred in the standard 5G standard compared to the 4G standard were obtained;
- variability over time is not only dependent on the communication standard used but also on the type of mobile application used;
- the self-similarity in the time variation of the signals depends on the communication standard used.

Study 4 – Use of statistical indicators and classification techniques with convolutional neural networks in the analysis of mobile phone signals in 4G and 5G communication standards

Materials and methods

As emission devices we used: mobile phone - iphone 14 pro (model A 2890, Apple, Zhengzhou, China) - for 4G emissions and mobile phone - iphone 13 (model A2633, Apple, Zhengzhou, China) - for 5G emissions- FR1. Monitoring of emitted power levels was performed for four types of applications running on the mobile phone: file upload, video streaming, file download and video call. Signal emission measurements were made using the following vector signal analyzers from Rhode&Schwarz: the FSV-3013 spectrum analyzer with

a real-time analysis bandwidth of 40 MHz (used for 4G signal measurements) and the FSW signal analyzer with a 160 MHz real-time analysis band (used for 5G signal measurements). To receive the signals, the Aaronia Omnilog 30800 (300-8000) MHz antenna with an omnidirectional characteristic in azimuth was used, positioned in all analyzed cases at a distance of 10 cm from the surface of the mobile phone, connected to the vector analyzer.

For 4G signals, the center frequency used was f1=1.75 GHz with a bandwidth of 20 MHz, and for signals broadcast in the 5G network, the center frequency used was f2=3.58 GHz with a bandwidth of 100 MHz . The receive antenna factor at both frequencies was extracted from the technical specifications provided by the supplier.

The algorithm presented in figure 8 includes all the experimental steps taken in order to measure and record the power level emitted by the mobile phones connected to the two mobile communication networks, determine the APD and CCDF parameters and retrieve the spectrograms related to the signals.

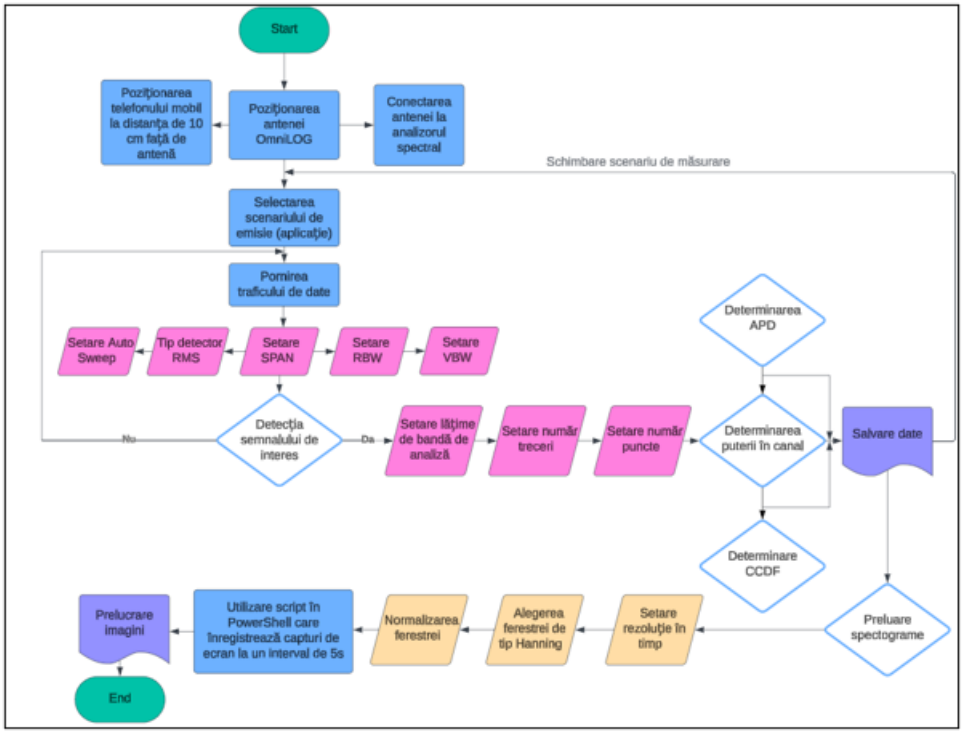

Figure 8 Algorithm for measuring and recording channel power, APD and CCDF parameters and signal spectrograms

In the present case, we focused the analysis on short-term variability and proposed the use of spectrograms and the deep-learning method in order to profile the exposure variability.

The use of convolutional neural networks provides traceability and insight into exposure dynamics by accurately recognizing and classifying emissions from different mobile communication technologies.

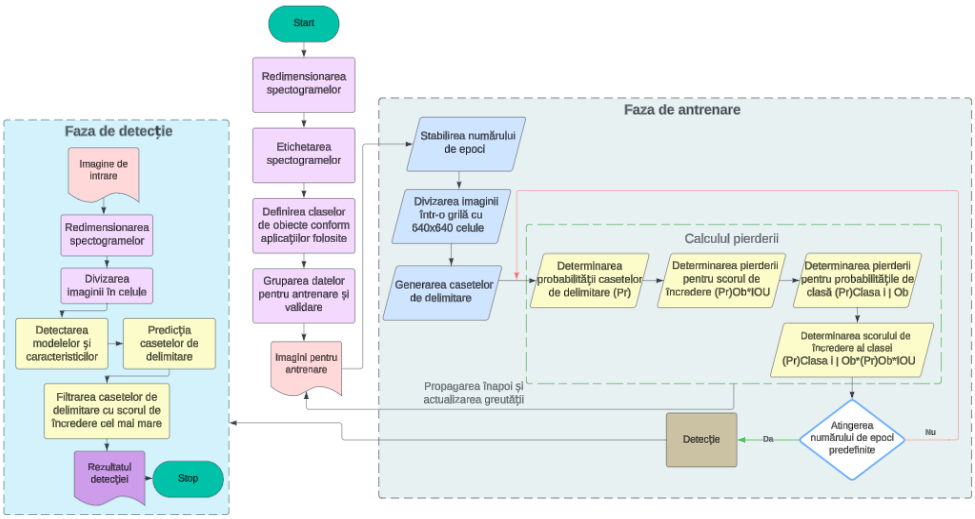

Figura 9 Organigrama proceselor de pregătire, antrenare și detecție a spectrogramelor aferente semnalelor 4G și 5G

Results and discussions

In order to accurately compare the APD function for those mobile networks, we measured the signals under similar conditions using similar settings. In the case of 4G signals, the shape of the curves for the file uploader application is different from the other applications (figure 10), being separated from them, a fact correlated with a higher probability of higher power levels. The video streaming and video calling applications show very similar power distributions, while the file uploader application shows high power emissions, although their probability of occurrence is consistently lower than for the file uploader application. Regarding the 5G standard, we note that the related emissions are much more similar to each other. The curves for file download and video call applications are almost similar, as are those for file upload and video streaming applications. Each of these two groups has similar probabilities of occurrence of the same power levels. Video calling and file downloading apps are almost twice as likely as file uploading and video streaming apps.

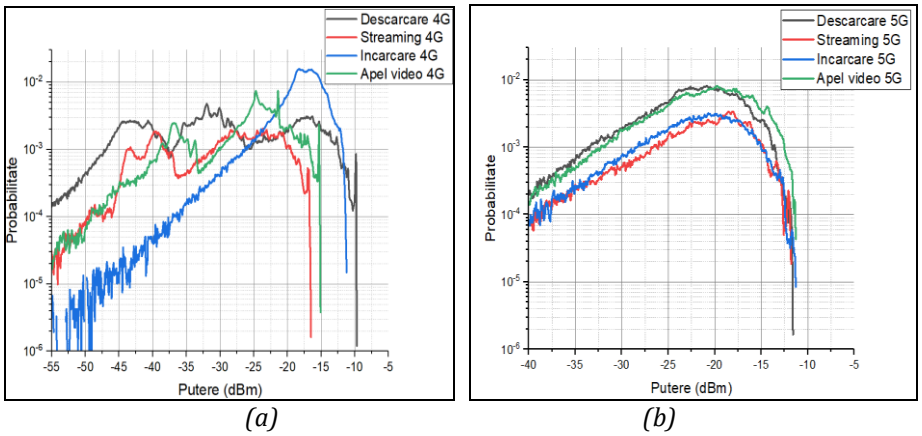

(a) *(b)*

Figure 10 Amplitude probability density (APD) of signals emitted at a distance of 10 cm from the surface of the mobile phone in the analysis bands for 4G and 5G networks: a) 4G – uplink signals; b) 5G – uplink signals

Following the analysis of the CCDF curves, the average crest factors and tails of the distribution for all mobile applications belonging to the same transmission technology were comparatively extracted. Crest factor values for 4G emissions are in the range (5-11) while

values for 5G-FR1 emissions are in the range (8.5-16.2). An important aspect can be highlighted in this case, namely the similarity between the crest factors for streaming and video calling mobile applications, in the two communication standards, 4G and 5G respectively, also indicating the use of similar modulations and coding schemes. On the contrary, the crest factor value for the file upload application is three times higher in 5G than in the 4G standard, while for the file download application, the crest factor is almost double in 5G than in 4G. This behavior can be explained as a result of the use of 256-QAM and 64-QAM modulations in the 5G standard for the two high field levels, as well as the highest data rates in a unit of transmission time.

The trend of extreme power values can be seen in Figures 11(b) and 12(b). We observe obvious differences in the distribution of powers between the two communication standards, as well as between mobile applications. The maximum overshoot of the average power in 5G compared to 4G belongs to the file upload application, having a value of 9.5 dB.

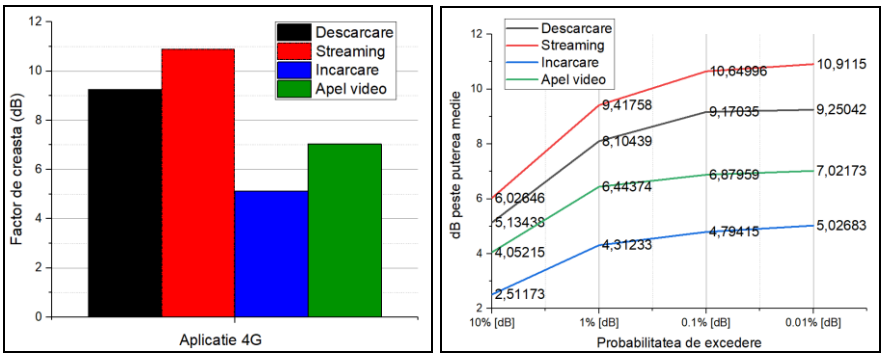

(a) *(b)*

Figure 11 Prevalence of peaks and highest power levels in 4G signal emissions: a) crest factors; b) the values of the highest percentages of power levels that exceed the average power

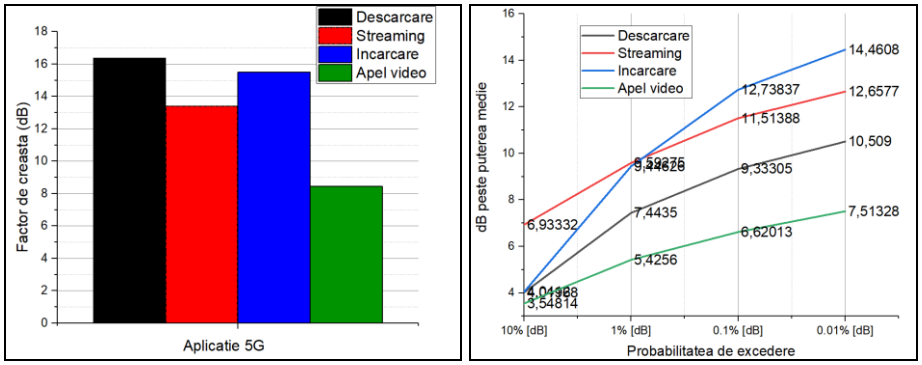

(a) *(b)*

Figure 12 Prevalence of peaks and highest power levels in 5G signal emissions: a) crest factors; b) the values of the highest percentages of power levels that exceed the average power

The power in the channel represents another indicator of human exposure to radio frequency sources, because based on its values and specific dynamics, we expressed the intensity and variability of the electric field at incidence with a hypothetical surface of a human body located at a distance of 10 cm. Figure 13 highlights the electric field intensities related to the five mobile applications used in the 4G standard (figure 13a) and in the 5G standard (figure 13b). The main observation in this case is represented by the fact that the emissions related to 5G technology are much higher than those related to 4G technology, also with notable differences between the four mobile applications. The standard deviations around the mean are the same for both communication standards, demonstrating a large variability in exposure. In 4G, the highest value of the electric field strength was found during

the use of the video calling application, while in 5G the maximum value was found for the video streaming application.

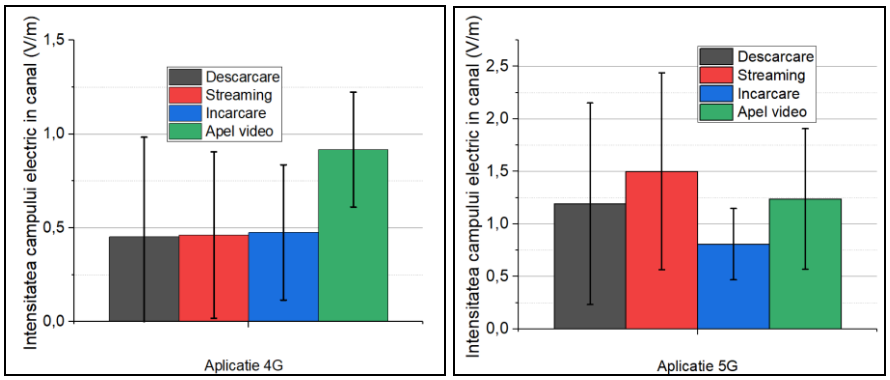

(a) *(b)*

Figure 13 The intensity of the electric field in the air, at a distance of 10 cm from the mobile phone, based on the measurements of the power in the channel – representations of the average value and standard deviation: a) 4G emissions; b) 5G emissions

After training the YOLO v7 algorithm with 300 spectrograms and validating it with 15 spectrograms, 10 spectrograms were used to identify and classify the respective emission. The success rate, as measured by the recognition rate, was very high, generally higher than 95%, with only one exception in the case of the Internet streaming application in the 4G standard where a low recognition rate of only 57% was recorded, according to figure 14a. Also, the Internet video streaming application was the most difficult to recognize in the 5G communication standard, although it had a high success rate (90%). For the 5G communication network (Figure 14b), higher uncertainties were identified than in the case of the 4G network, which are indicated by the existence of error bar lengths.

By proper manual setting, the prepared spectrograms were classified with a high success rate using the YOLO v7 algorithm, even though the training and validation was performed on a small number of samples. Therefore, YOLO v7 proved to be a useful and very powerful algorithm in recognizing features related to power spectrum variability.

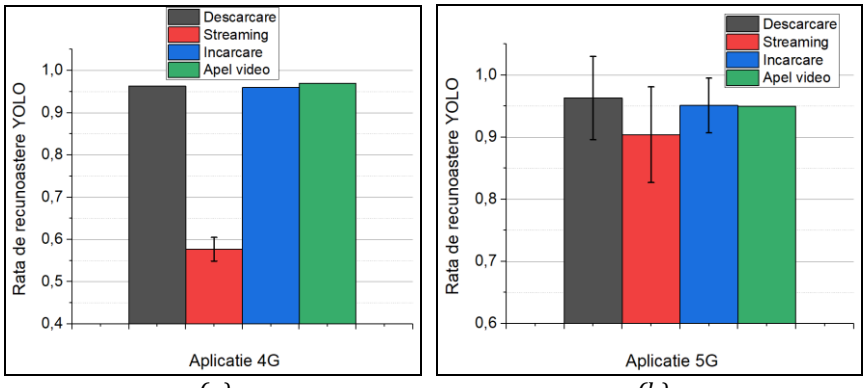

(a) *(b)*

Figure 14 Recognition rate of mobile applications using the YOLO v7 algorithm for: a) 4G emissions; b) 5G emissions

Conclusions

Among the main characteristics identified in this study we list: higher electric field intensity values for 5G-FR1 signal emissions compared to 4G emissions, no electric field intensity values were recorded that exceeded the exposure limits established by the regulations in force, the prevalence of the highest power levels was more frequent for 5G-FR1

emissions than for 4G emissions, and the recorded spectrograms revealed significant differences between the mobile applications used.

Study 5 – Evaluation of the impact of 5G-FR1 signals on the user: The influence of the phase difference between the elements of phased microstrip antenna arrays on the spatial distribution of the incident electric field and the specific energy absorption rate

Materials and methods

Microstrip antennas are the most widely used antenna types in mobile terminal and router configuration in indoor environments due to easy replication, low cost and low profile. All simulations were performed within the CST MWS Studio software program using the finite integration technique (FIT). Within the program CST Microwave Studio, two types of planar arrays of microstrip antennas were modeled, namely: 1x4 element and 2x4 element phased antennas at the operating frequencies of 3.7 GHz and 5.8 GHz. The 3.7 GHz frequency is usually used for access points in the indoor environment, devices often found in various locations where people are present, and the 5.8 GHz frequency is part of the 5 GHz Wifi spectrum.

The configuration of the phased antennas modeled in the simulation program, as well as their constructive parameters can be seen in figures 15-16.

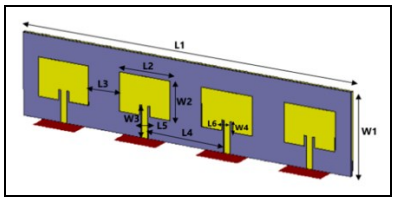

Denumire parametru	Valoare (mm)
L1	160
L2	24.94
L3	15.34
L4	37
L5	3
L6	1
W1	40
W2	19.20
W3	15.58
W4	5

(a)

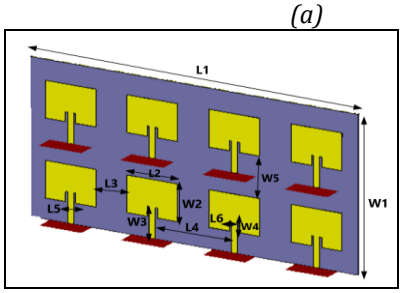

Denumire parametru	Valoare (mm)
L1	160
L2	24,94
L3	15,34
L4	37
L5	2,745
L6	1
W1	80
W2	19.20
W3	15.58
W4	5
W5	21,15

(b)

Figure 15 Configuration of antenna arrays: a) with 1x4 elements at the resonance frequency 3.641 GHz; b) 2x4 elements at the resonance frequency 3.692 GHz and their constructive parameters

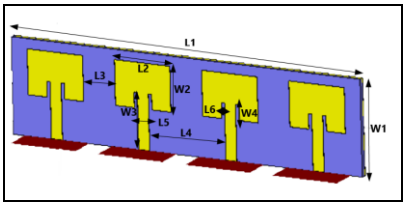

Parametru	Valoare (mm)
L1	100
L2	15,82
L3	9,12
L4	22
L5	2,74
L6	1
W1	25
W2	11,94
W3	14,5
W4	4

(a)

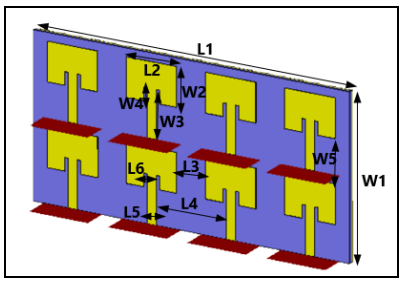

Parametru	Valoare (mm)
L1	100
L2	15,88
L3	9,12
L4	22,10
L5	2,74
L6	1
W1	50
W2	11,99
W3	14,56
W4	4
W5	13,12

(b)

Figure 16 Configuration of antenna arrays: a) with 1x4 elements at the resonant frequency 5.802 GHz; b) 2x4 elements at the resonance frequency 5.797 GHz and their constructive parameters

The phased plane antennas were successively positioned at a fixed distance of 20 cm from the head model (figure 17).

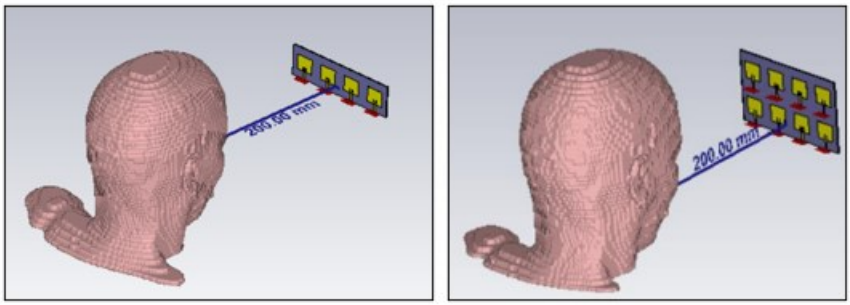

Figure 17 Exposure scenario: a) microstrip antenna with 1x4 phased elements; b) microstrip antenna with 2x4 phased elements

In this study we calculated the intensity of the incident electric field on the tangent plane of the head, in air and the specific absorption rate for the head model for the four types of modeled phased antennas. To thoroughly analyze the distribution of SAR values inside the head, we chose a plane of section vertical to the head model, which marks a section through its center (sagittal plane). We also extracted the peak values, SARmax(10g) – averaged over 10g tissue and the mean values, SARmean(10g) in each tissue (skin, fat, muscle, bone, brain and eye tissue) depending on the phase difference used between the elements of phased antennas (different direction angle of the antenna beam).

Results and discussions

Analysis of the influence of the phase difference between the elements of the 1x4 element antenna array at the frequency of 3.641 GHz on the specific energy absorption rate (SAR)

In order to determine the impact of the phase difference between the elements of the antenna array, on its performance as well as on the exposed head model, we simulated various specific cases where the antenna array has the four elements out of phase. The cases addressed can be found in table 1. Based on the results obtained, we note that if there is no phase shift between the elements of the antenna array, a sufficiently high gain is obtained compared to other cases, but not the highest. So the maximum gain of an antenna array can also be improved by applying special phase differences between its elements. In this sense for the case [0;30;80;130] the maximum gain of 6.95 dBi was obtained. However, for this type of phased array antenna, low gain values were also obtained at the resonance frequency of 3.641 GHz. For example, it is observed that for a phase difference of 180 degrees between the

antenna elements, the performance and constructive properties of the antenna array decrease considerably, obtaining a gain of 2.74 dBi.

Table 1 The influence of the phase difference between the elements of the microstrip antenna array with 1x4 elements on its main parameters

Phase difference	Maximum antenna gain (dBi)	Total efficiency (dB)
[-30;0;0;30]	6,86	-3,848
[-60;0;0;60]	6,61	-4,141
[-90;0;0;90]	6,27	-4,196
[-180;0;0;180]	5,14	-3,998
[0;0;0;0]	6,81	-3,847
[0;30;80;130]	6,95	-3,905
[20;80;100;150]	6,84	-4,000
[30;0;30;0]	6,5	-3,941
[40;180;60;270]	3,86	-5,345
[60;0;60;0]	5,67	-4,262
[60;90;180;270]	**6,91**	-3,823
[90;0;90;0]	4,43	-4,783
[180;0;180;0]	2,74	-6,198
[270;0;270;0]	4,59	-4,944
[270;30;90;180]	6,5	-3,903

In order to analyze the electric field intensity distribution in the case of using the antenna array with 1x4 elements, I chose a plane parallel to it, at a distance of 20 cm, located in close proximity to the head model. Thus in figure no. 18 the planes parallel to the array of antennas related to each phase difference can be observed. The scale of values includes all values of the electric field in that plane, between the minimum value and the maximum value. For the [180;0;0;180] case, the lowest value of the electric field intensity was obtained, namely 18 V/m, because the antenna array has the lowest efficiency. The maximum value of the electric field strength - 63.5 V/m was identified in case [0;0;0;0]. Although in this case the highest gain of the antenna array was not obtained, the maximum value of the electric field was obtained, so we can state that using the phase difference between the elements of an antenna with a high gain does not lead to the highest values values of E (V/m).

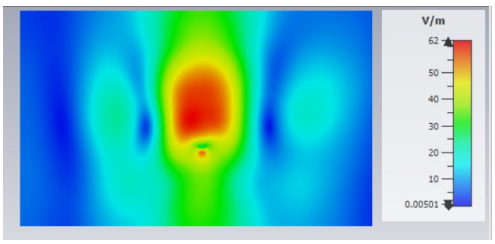

[-30;0;0;30]

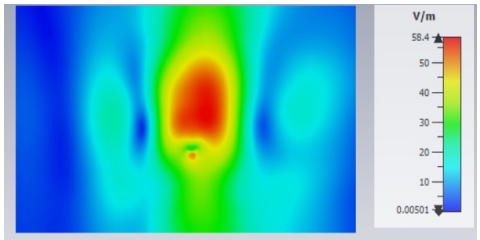

[-60;0;0;60]

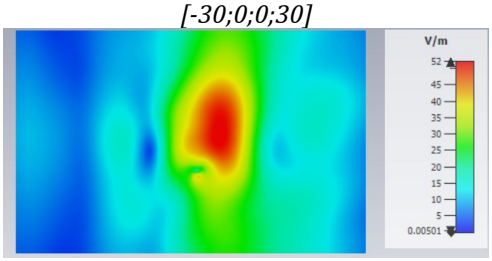

[-90;0;0;90]

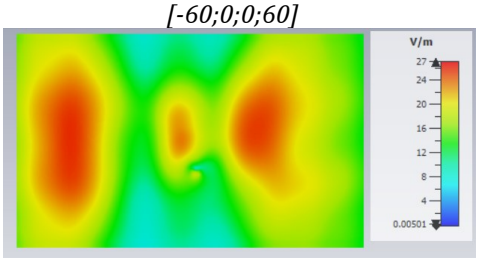

[-180;0;0;180]

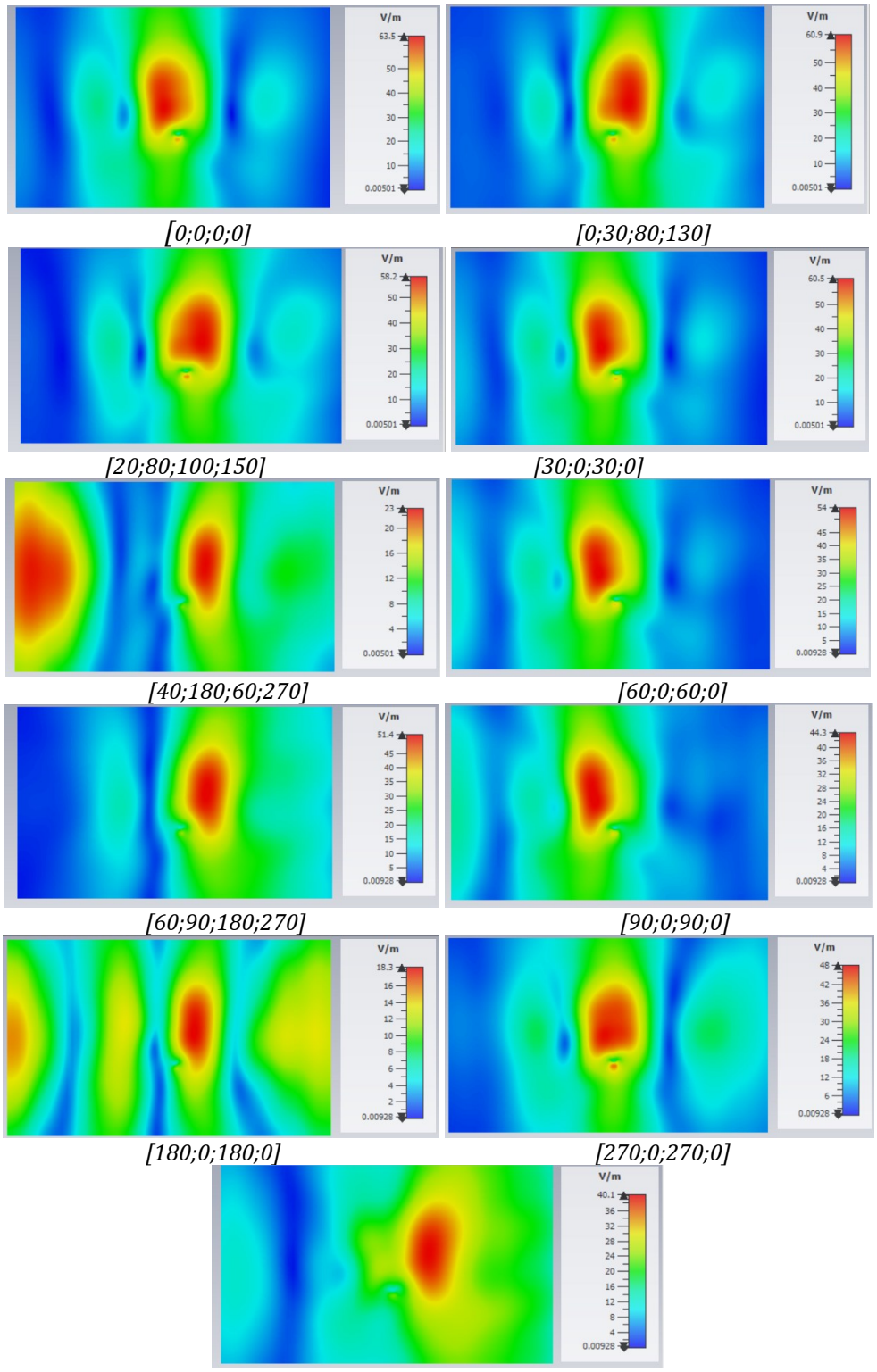

Figure 18 Distribution of the electric field intensity in a plane parallel to the antenna of 1x4 elements, at the distance of 20 cm (tangent to the face of the head model) according to the phase differences between the antenna elements

For a more thorough analysis of the distribution of SAR values, we chose a plane of section parallel and horizontal to the head model, which marks a section through its center, according to figure no. 19 SARmax was identified when using the phase difference [-30,0,0,30], because the main radiation lobe is positioned on the radiation diagram (located at 5 degrees distance) closest to the main direction (0 degrees) on which the head model is

located. Also, the radiation lobe is the narrowest, with an angular width of 12 degrees, being much more directional. Although we obtained the highest gain of the antenna in the case of using the phase difference [0,30,80,130], the SARmax has a low value of 1.89e-5 W/kg, which can be explained by the fact that as the angular width of the main radiation lobe increases, it is less directive, and the amount of transmitted power is concentrated over a much larger area.

We notice that the SAR distribution is completely different for the cases [0,30,80,130], [40;180;60;270], [60;0;60;0] and [270;0;270;0] compared to the others . This is primarily due to the fact that the angular width of the main radiation lobe is large and secondly because it is oriented in a direction that does not coincide with the normal incidence on the head model surface.

According to the graphs, the highest SAR values are found in the following tissues: skin, fat and eyes.

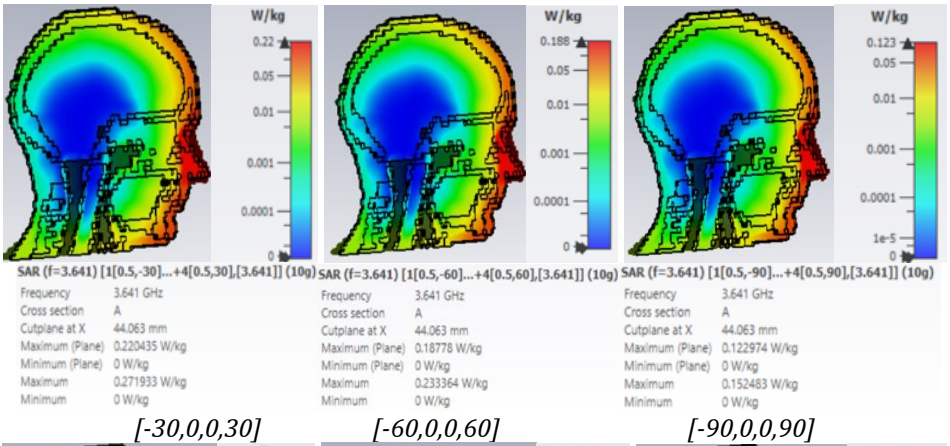

[-30,0,0,30] *[-60,0,0,60]* *[-90,0,0,90]*

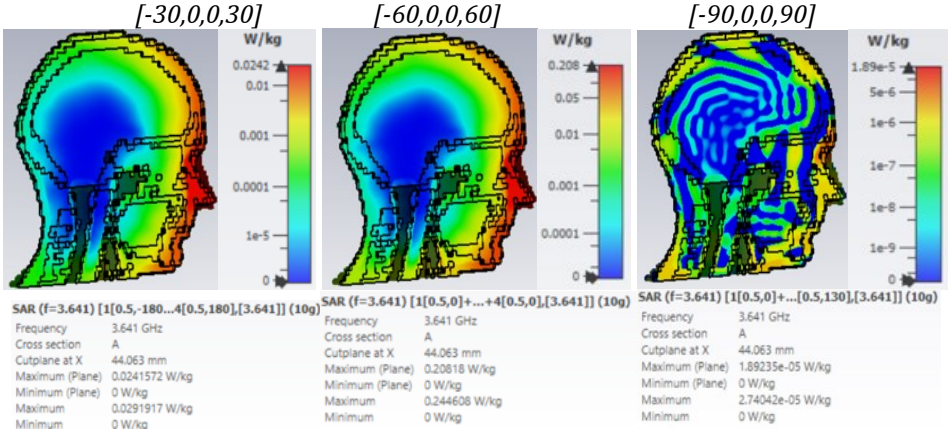

[-180,0,0,180] *[0,0,0,0]* *[0,30,80,130]*

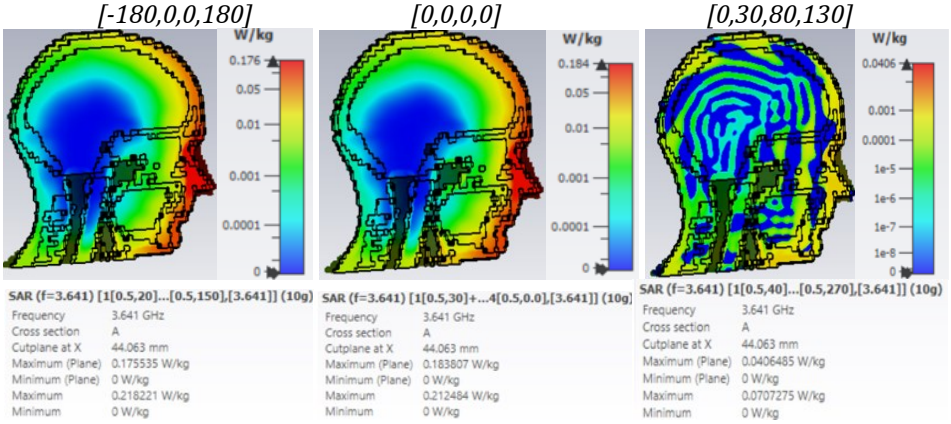

[20;80;100;150] *[30;0;30;0]* *[40;180;60;270]*

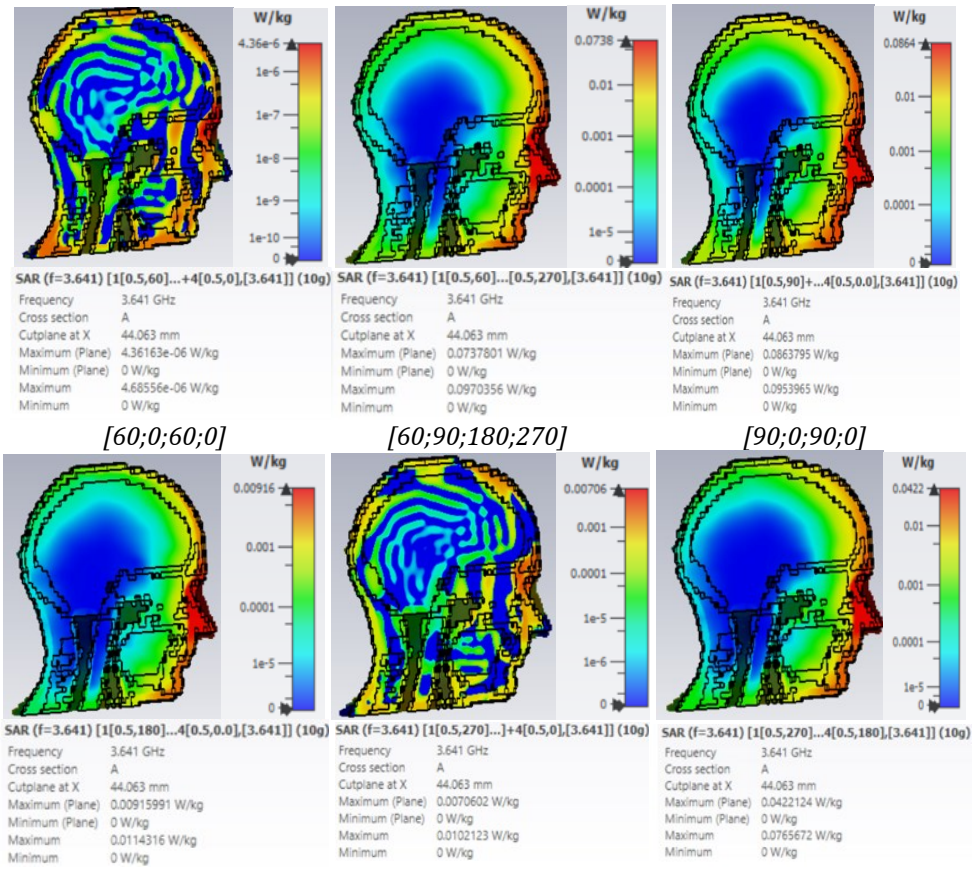

Figure 19 Distribution of SAR10g (W/kg) in a vertical plane through the center of the head pattern for the 1x4 antenna array as a function of the phase difference between its elements

In the following two graphs, figure 20 and figure 21, we have plotted the SARmax(10g) and SARmean(10g) values from each tissue according to the phase difference used between the phased antenna elements. In this sense, for SARmax the values have a linear tendency to decrease, according to the transition from one tissue to another, from the outside to the inside. Skin and fat tissues absorb an approximately equal amount of energy, even in muscle and bone tissue we observe the presence of SAR. In the brain the SARmax values are in the range [3.55e-05.0556W/kg]. According to the two graphs, the eye tissue absorbs a considerable amount of energy because the associated electrical permittivity is low and the exposed tissue surface is small. We identify the highest SAR max values in the following cases: [-30,0,0,30], [0,0,0,0], [-60,0,0,60].

The SARmax values identified for this exposure case do not exceed the exposure reference limits established in the ICNIRP 2020 guidelines.

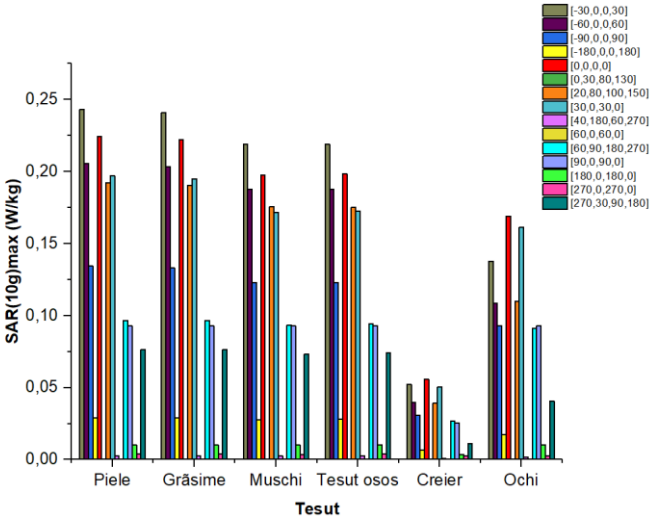

Figure 20 SAR (10g)max (W/kg) inside each tissue as a function of the phase difference used between the elements of the 1x4 antenna array

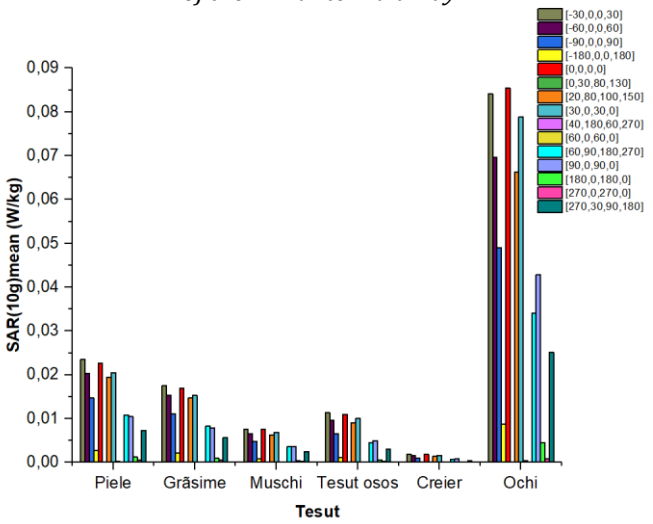

Figure 21 SAR (10g)mean(W/kg) inside each tissue as a function of the phase difference used between the elements of the 1x4 antenna array

Analysis of the influence of the phase difference between the elements of the 2x4 element antenna array at the frequency of 5.797 GHz on the specific energy absorption rate (SAR)

In Table 2 we kept the same cases for the phase differences originally used in the case of the 3.7 GHz frequency for the same type of antenna configuration. We observe the maximum value of gain and efficiency for simulation case no. 6, and the minimum values of the two parameters were identified for simulation no. 9. The previous simulations, together with the one related to this case, confirm that the use of the 180 degree phase between the antenna elements leads to the lowest antenna performance, in most cases as well as at the lowest values of E (V/m) and SAR (W/kg).

Table 2 The influence of the phase difference between the elements of the microstrip antenna array with 2x4 elements on its main parameters

Phase difference	Maximum antenna gain (dBi)	Total efficiency (dB)	Obs.
[0;0;0;0;0;0;0;0]	8,74	-4,56	Simulare 1
[-180;0;180;0;-180;0;180;0]	5,41	-4,42	Simulare 9

[-30,0;30;0;-60;0;60;0]	7,77	-4,35	Simulare 10
[30;60;90;120;150;180;210;230]	4,34	-5,53	Simulare 4
[270;90;300;60;330;30;120;0]	4,81	-4,97	Simulare 11
[-30;-60;-90;-120;-150;-180;-210;-240]	9,44	-3,67	Simulare 6
[150;-80;-10;60;130;200;270;340]	**9,85**	-3,61	Simulare 12
[0;-30;-60;-90;90;60;30;0]	8	-5,19	Simulare 13
[90;0;-90;0;30;0;-30;0]	7,67	-4,26	Simulare 14

Compared to the distribution of the electric field intensity values specific to the antenna arrays used at resonance frequencies, in this case, being the only one, we observe a concentric structure of it for all the phase differences used. So the amount of radiation is concentrated on small and narrow surfaces, tending to propagate from the inside to the outside of the reference sectional plane, and depending on the phase chosen, it is denser either on the right side, on the left side or on both sides of the plan.

We also identify much larger surfaces, where the radiation is concentrated, as well as higher values of the electric field intensity. In this sense, we determined the maximum value of 170 V/m in the case of simulation 12, and the minimum value of 44.9 V/m in the case of simulation 9. For this studied case, the highest values of the electric field intensity were recorded for certain differences of phase compared to the three previous studies.

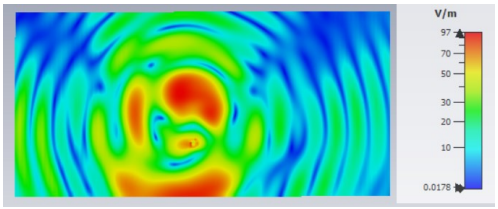

[0;0;0;0;0;0;0;0]

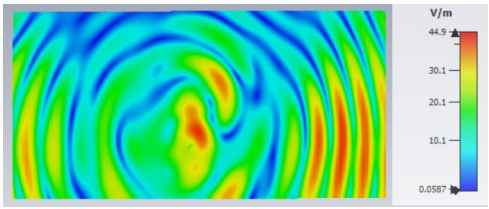

[-180;0;180;0;-180;0;180;0]

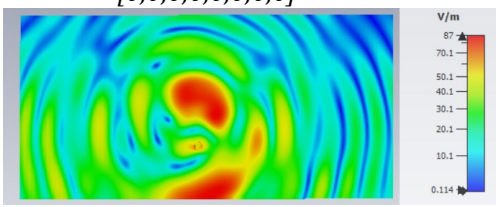

[-30,0;30;0;-60;0;60;0]

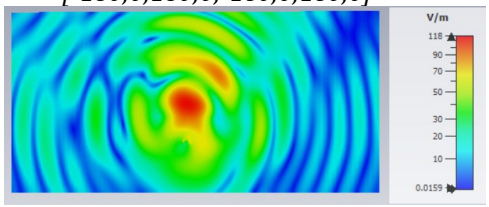

[30;60;90;120;150;180;210;230]

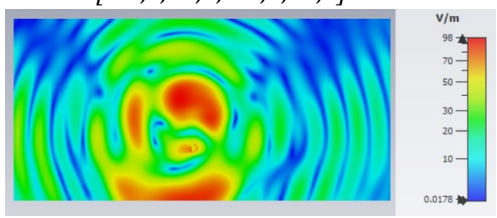

[270;90;300;60;330;30;120;0]

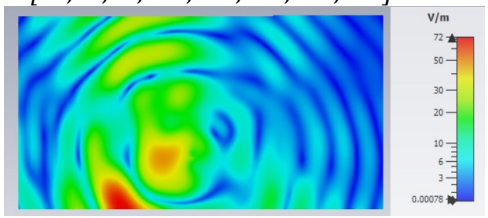

[-30;-60;-90;-120;-150;-180;-210;-240]

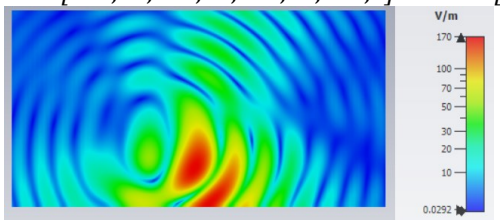

[-150;-80;-10;60;130;200;270;340]

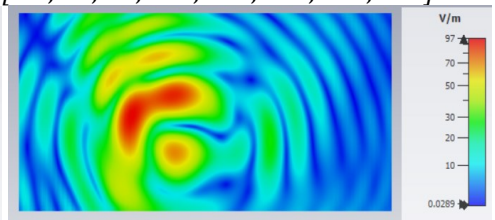

[0;-30;-60;-90;90;60;30;0]

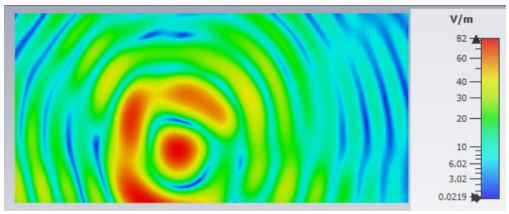

[90;0;-90;0;30;0;-30;0]

Figure 22 Distribution of the electric field intensity in a plane parallel to the 2x4 element antenna, at a distance of 20 cm (tangent to the face of the head model) according to the phase differences between the antenna elements

As the antenna configuration changes, differences are observable regarding the SAR distribution, in this sense for simulations 1, 9, 10, 11 and 13 the radiated energy is concentrated more in the area of the nose, eyes, mouth and neck compared to simulation 4 where radiation is present in the forehead and nose area. These differences occur in terms of phase shift, as well as antenna and tissue characteristics. In the reference plane that cuts the head model, for simulation 1 we identify the maximum value of SAR (0.617 W/kg), for the same simulation the maximum values of SAR were also recorded in the case of the antenna with 2x4 elements at the frequency of 3.692 GHz. The minimum value of the specific absorption rate (0.0641 W/kg) can be seen in the image specific to simulation 9.

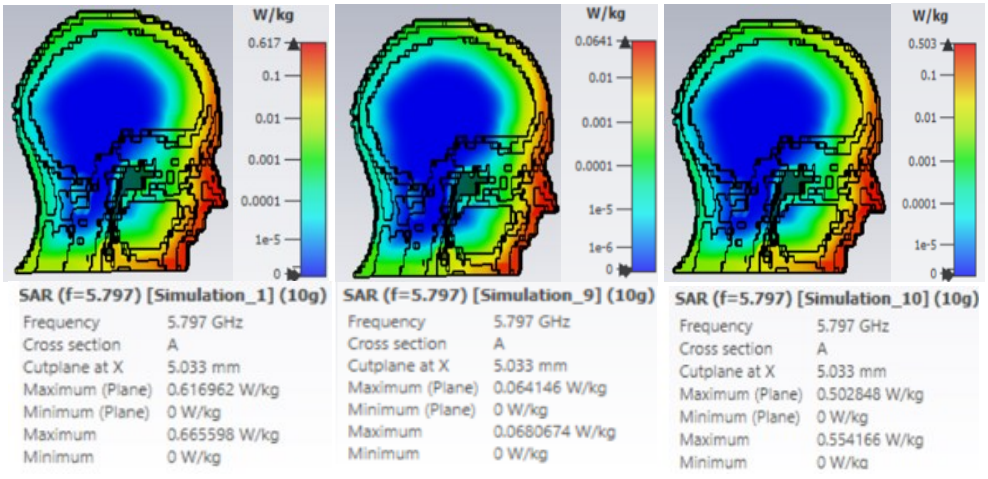

Simulare 1 *Simulare 9* *Simulare 10*

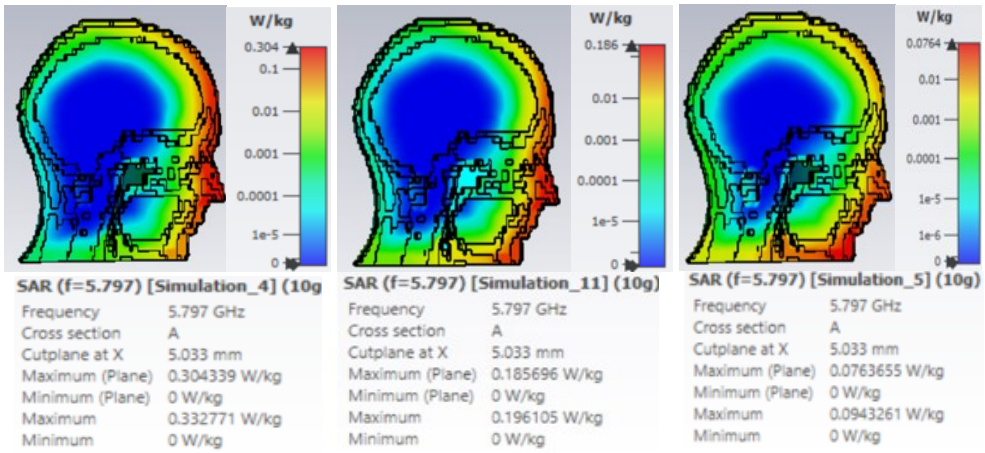

Simulare 4 *Simulare 11* *Simulare 5*

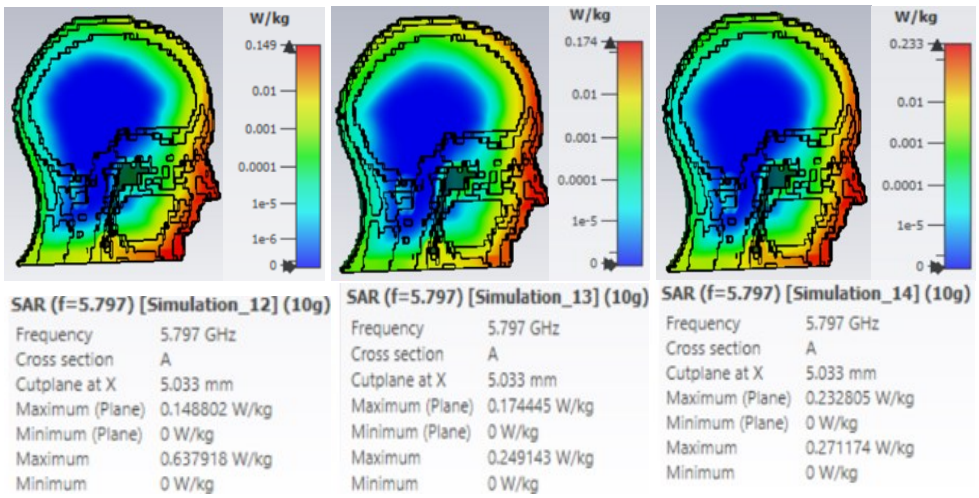

Simulare 12 *Simulare 13* *Simulare 14*

Figure 23 Distribution of SAR10g (W/kg) in a vertical plane through the center of the head pattern for the 2x4 antenna array as a function of the phase difference between its elements

In the graph related to figure 24 for the cases [0,0,0,0,0,0,0,0,] and [-150,-10,60,130,200,270,340] the highest SARmax values were recorded at the level of skin and fat tissues . And in this case, the specific absorption rate indicates higher values in the bone tissue than in the muscle tissue, an identical aspect for the SARmean values. For the 5.8 GHz frequency, this type of antenna configuration leads to the highest SARmean and SARmax values.

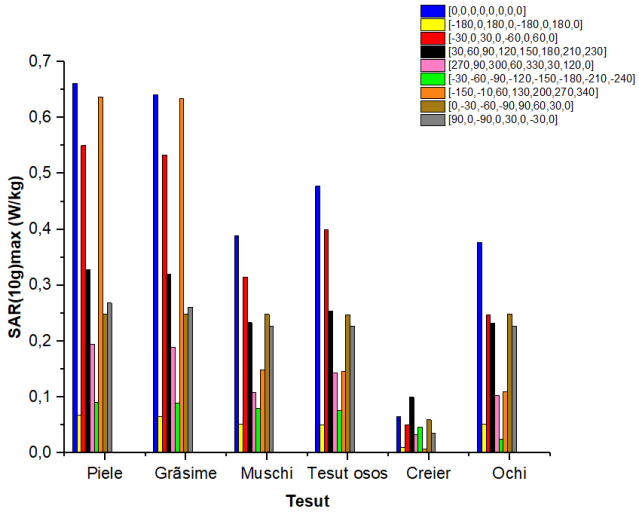

Figure 24 SAR (10g)max(W/kg) inside each tissue as a function of the phase difference used between the elements of the 2x4 antenna array

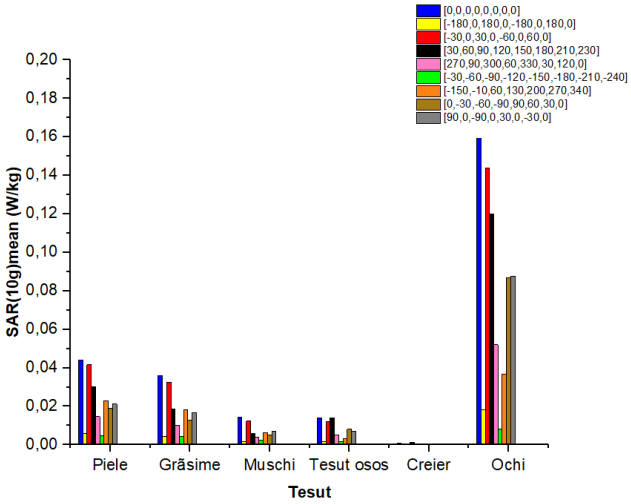

Figure 25 SAR (10g)mean(W/kg) inside each tissue as a function of the phase difference used between the elements of the 2x4 antenna array

Conclusions

Given the fact that in the study, lower specific absorption rate values were obtained than those established in the ICNIRP standard, we can state that the four evaluated exposure situations respect the safety limits from the point of view of exposure to radiofrequency sources. In contrast, specific points were identified inside and outside the head model where the local SAR value was significant, which can lead to the appearance of intense "hot spots". These cases were found in skin, fat and eye tissue. We also observed that exposure levels change dramatically depending on the direction of the radiation beam, for example radiation lobes that are perpendicular to the surface of the head model produce high values of electric field strength and specific absorption rate over time which lobes oriented in other directions assume lower values of these parameters.

Final conclusions

The exposure of biological matter to electromagnetic radiation generated by communication systems is an ongoing concern and of scientific interest worldwide. Evaluation and analysis of the temporal variability of these electromagnetic fields are essential in order to corroborate the dose-effect or dose-rate-threshold effect. As a result of the impressive increase in the number of communication systems, including networks and mobile phones and Wi-Fi equipment, and as a result of the development of the 5G communication network, the need for a detailed analysis of the emissions generated by such equipment, especially under the aspect of identifying temporal "fingerprints", including the characterization of probability distributions of amplitudes, crest factors and recurrences in the emission time series. The present research investigated in various scenarios the dynamics of the signals emitted in the 4G and 5G communication standards through comprehensive studies but also through comparison, in order to identify the exposure and dosimetry peculiarities.

Given the fact that the main sources of exposure are represented by base station antennas of cellular communication networks and mobile phones, the present approach was focused on characterizing the emissions generated by such systems. In this sense, in the first part of the research, a study was carried out regarding the monitoring and evaluation of the

electromagnetic environment by using the data collected by the fixed monitoring stations of the national broadband monitoring system (100 kHz – 7 GHz) implemented by ANCOM. Various statistical methods were therefore used for the first time for the analysis of temporal variations and the identification of particularities in the temporal nature of electromagnetic field levels. Later the research was extended by evaluating the time-print of emissions from base stations and mobile phones, including with the help of recurrence analysis which until now has only been used in the characterization of biomedical, acoustic, economic, financial, neural and climate signals. Therefore, within the time series of the analyzed field levels, hidden recurrent patterns and structural changes were determined that could not be highlighted by classical methods of signal analysis.

The following approach consisted of two studies that were oriented to the detailed analysis of the emitted field dynamics near mobile phones connected to commercial 4G and 5G networks. In this sense, various metrics and methods have been validated in the detailed analysis of the amplitude-time variability of the signals emitted by mobile phones.

The last part of the research complements the previous exposure studies with a numerical dosimetric study to evaluate the impact of 5G-FR1 signals on the human body (head) and the influence of the use of beamforming and beamsteering techniques on the spatial distribution of the incident electric field and the specific absorption rate of energy. The study was focused on highlighting the variation of the absorbed power – both in terms of amplitude level and positioning in the head areas, depending on the phased antenna arrays designed for adaptive beamforming. At each variation of the beam steering angle and depending on each antenna design, different doses of radiation were delivered to the same tissue.

The present work provides a complementary picture, extremely undervalued in the literature, on the amplitude-time peculiarities of emissions from cellular network base stations and mobile phones, by successfully applying accurate measurement methods and processing procedures advanced data in order to characterize and forecast the exposure footprint of emissions. The results obtained in this doctoral thesis contribute to the identification of the connections between the speed of change of the electromagnetic stimulus and the threshold for triggering a specific biological effect, post-exposure.

PhD thesis contributions

The following contributions of the PhD thesis in the field of research are relevant:

a) Evaluation and interpretation in relation to the reference levels imposed by the regulations in force of the electric field intensity values measured by fixed electromagnetic field monitoring systems, over a period of one year, in seven urban sub-areas in the city of Bucharest. The database was made up of over 2 million samples. At the same time, a comparative analysis of the level of exposure of the population in the first quarter of 2024 compared to the first quarter of 2023 was carried out. The element of novelty in this experimental study was represented by the use of statistical analysis methods that allowed the extraction of some behaviors " hidden" of the emitted signals.

b) The use of noise-immune recurrence analysis methods in order to determine and characterize the dynamic-recursive behavior of signals emitted by base stations and mobile phones. At the same time, a comparative analysis of the emissions generated by the two categories of communication systems was carried out.

c) Evaluation of exposure to radiation emitted in the near field of a mobile terminal successively connected to 4G and 5G communication networks. The experimental evaluation of the dynamics of the radiated field near a mobile phone while running five different mobile applications aimed to identify and highlight the particularities of electromagnetic exposure, as well as differences between the time variation of the field emitted by the two communication standards.

d) Approaching a complementary characterization of human exposure through the energy fluence rate adapted to the frequency range in the GHz range. Based on this quantity, it has been shown that a prediction is possible based on the differentiation between chaotic and random emissions of 4G and 5G signals, evidenced by temporal recurrence quantification.

e) Evaluation of the impact of the introduction of the new 5G communication systems on the human exposure profile and the capitalization of the temporal "footprint" of the distribution of the amplitudes emitted during the use of the mobile phone.

f) Evaluation of probability densities of amplitudes, exposure accumulation rates, crest factors and statistical distributions of amplitudes for 4G and 5G signals, comparatively, from the perspective of corroboration with trigger levels of a specific biological effect.

g) The use of an algorithm based on convolutional neural networks in order to classify the signal emissions for four types of mobile applications run in the 4G and 5G communication standards in order to identify the particularities related to the connection used and the distribution mode of the emitted power.

h) Implementation, testing and evaluation of beamforming and beamsteering performances at the level of modeled adaptive antennas. Much more directional and narrow radiation lobes were obtained as the number of elements increased in the patterned antenna array configuration to operate at 3.7 GHz and 5.8 GHz frequencies. It has also been noted that the performance of an antenna is improved as certain phase differences are applied between its elements.

i) Identification of the spatial variability of human exposure as a result of the use of beamforming and beamsteering techniques within emission sources. In this sense, we identified that the radiation lobes that are perpendicular to the surface of the human head model produced high values of the intensity of the incident electric field and of the specific rate of energy absorption, compared to the lobes oriented in other directions.

j) Determination of the values of the specific absorption rate and the level of the electric field intensity for different scenarios of exposure of the Laura physical model of the human head to the radiation emitted by adaptive antennas at 3.7 GHz and 5.8 GHz frequencies.

k) The use of the technique of adaptive formation of radiation beams, as well as directing them in certain directions did not lead to obtaining the highest values of the intensity of the electric field, in this sense it can be stated that the new methods used in 5G

communication technology do not contribute automatically when the exposure level increases. Compared to the situation of in-phase feeding of the antenna elements, where the highest values of the specific absorption rate were obtained, in the case of introducing the phase difference between the antenna elements, lower SAR values were obtained.de fază între elementele antenei au fost obținute valori mai reduse ale SAR.

l) Identification of significant SAR values and "hot spots" in the skin, fat and eye tissue.

REFERENCES THESIS

[1] Mahmud, H. (2019). Cellular Mobile Technologies (1G to 5G) and Massive MIMO. *International Journal of Science and Research (IJSR)*, vol. 8, pp. 929–937.

[2] Bandi, A. (2022). A Review Towards AI Empowered 6G Communication Requirements, Applications, and Technologies in Mobile Edge Computing. *2022 6th International Conference on Computing Methodologies and Communication (ICCMC)*, pp. 12–17.

[3] Patel, S., Shah, V., & Kansara, M. (2018). Comparative Study of 2G, 3G and 4G. *International Journal of Scientific Research in Computer Science, Engineering and Information Technology*, vol. 3, pp. 1962- 1964.

[4] Sauter, M. (2014). Global System for Mobile Communications (GSM)" in *From GSM to LTEAdvanced: An Introduction to Mobile Networks and Mobile Broadband*, Wiley, pp. 1-71.

[5] Sikora, A., Yunitasari, A., & Dold, M. (2013). GPRS and UMTS services for ultra low energy M2M-communication. *2013 IEEE 7th International Conference on Intelligent Data Acquisition and Advanced Computing Systems (IDAACS)*, pp. 494–498.

[6] Richardson, K. W. (2000). UMTS Overview. *Electronics & Communication Engineering Journal*, vol. 12, no. 3, pp. 93-100.

[7] Holma, H., Toskala, A., & Tapia, P. (2014). HSPA+ Evolution to Release 12: Performance and Optimization, Wiley, pp. 421-431.

[8] System Architecture Evolution. (2013) in *LTE and the Evolution to 4G Wireless: Design and Measurement Challenges,"* Agilent Technologies, Wiley, pp. 195-228.

[9] Navarro-Ortiz, J., Romero-Diaz, P., Sendra, S., Ameigeiras, P., Ramos-Munoz, J. J., & Lopez-Soler, J. M. (2020). A Survey on 5G Usage Scenarios and Traffic Models. *IEEE Communications Surveys & Tutorials*, *22*(2), 905–929.

[10] Ismail, L., & Buyya, R. (2022). Artificial Intelligence Applications and Self-Learning 6G Networks for Smart Cities Digital Ecosystems: Taxonomy, Challenges, and Future Directions. *Sensors*, *22*(15).

[11] 3GPP (3rd Generation Partnership Project). Technical Specification Group Radio Access Network; Evolved Universal Terrestrial Radio Access (E-UTRA); Physical Layer Procedures (Release 15). *3GPP TS 36.213*.

[12] Bucur, C. (2015). Comunicaţii mobile, Editura Universităţii Petrol – Gaze din Ploieşti, pp. 115-136.

[13] Mountassir, J., Balta, H., Kovaci, M., & Isar, A. (2011). Study of multiple access schemes in 3GPP LTE OFDMA vs. SC-FDMA. *International Conference on Applied Electronics*, pp. 1-4.

[14] Cox, C. (2014). An Introduction to LTE: LTE, LTE-Advanced, SAE, VoLTE and 4G Mobile Communications, Wiley, pp. 67-75.

[15] William C. Y. Lee. (1998). *Mobile Communications Engineering: Theory and Applications, Second Edition* (Second Edition). McGraw-Hill Education.

[16] Grami, A. (2015). *Introduction to digital communications*. Academic Press.

[17] Stefanovic, N., Blagojevic, M., Pokrajac, I., Greconici, M., Cen, Y., & Mladenovic, V. (2020). A Symbolic Encapsulation Point as Tool for 5G Wideband Channel Cross-Layer Modeling. *Entropy*, *22*(10).

[18] Han, M. S., Lee, J. W., Kang, C. G., & Rim, M. J. (2019). System-level Performance Evaluation with 5G K-SimSys for 5G URLLC System. *2019 16th IEEE Annual Consumer Communications & Networking Conference (CCNC)*, pp. 1–5.

[19] Hassani, S. E., & Haidine, A. (2015). Roadmap towards beyond 4G: Key technologies and challenges for 5G. *2015 International Conference on Wireless Networks and Mobile Communications (WINCOM)*, pp. 1–6.

[20] Vihriälä, J., Zaidi, A. A., Venkatasubramanian, V., He, N., Tiirola, E., Medbo, J., Lähetkangas, E., Werner, K., Pajukoski, K., Cedergren, A., & Baldemair, R. (2016). Numerology and frame structure for 5G radio access. *2016 IEEE 27th Annual International Symposium on Personal, Indoor, and Mobile Radio Communications (PIMRC)*, pp. 1–5.
[21] Patriciello, N., Lagén, S., Giupponi, L., & Bojović, B. (2018). 5G New Radio Numerologies and their Impact on the End-To-End Latency. *2018 IEEE 23rd International Workshop on Computer Aided Modeling and Design of Communication Links and Networks (CAMAD)*, pp. 1–6.
[22] Bag, T., Garg, S., Shaik, Z., & Mitschele-Thiel, A. (2019). Multi-Numerology Based Resource Allocation for Reducing Average Scheduling Latencies for 5G NR Wireless Networks. *2019 European Conference on Networks and Communications (EuCNC)*, 597–602.
[23] Bertenyi, B. ., Nagata, S. ., Kooropaty, H. ., Zhou, X. ., Chen, W. ., Kim, Y. ., Dai, X. ., & Xu, X. . (2018). 5G NR Radio Interface. *Journal of ICT Standardization*, *6*(1-2), pp. 31–58.
[24] Prasad, K. N. R. S. V., Hossain, E., & Bhargava, V. K. (2017). Energy Efficiency in Massive MIMO-Based 5G Networks: Opportunities and Challenges. *IEEE Wireless Communications*, *24*(3), pp. 86–94.
[25] Lecture 15 – EE 359, "MIMO Systems: Channel Capacity, Beamforming, Diversity-Multiplexing Tradeoff and RX Design," in Wirel. Commun. Lect. Notes, 2016. Preluat de pe web.stanford.edu:
https://web.stanford.edu/class/ee359/previous/pdfs/lecture15_handout.pdf
[26] Zhou, I., Ramírez, G. A., Montero, L., Blanch, S., Romeu, J., & Jofre, L. (2020). Three-Dimensional Beamsteering Low-Complexity Reconfigurable Multilevel Antenna. *IEEE Antennas and Wireless Propagation Letters*, *19*(6), pp. 1017–1021.
[27] 3GPP (3rd Generation Partnership Project). 5G; NR; User Equipment (UE) procedures in idle mode and in RRC inactive state (version 16.1.0 release 16). *3GPP TS 38.304*
[28] 3GPP (3rd Generation Partnership Project). Study on new radio access technology Physical layer aspects (version 14.2.0). *3GPP TR 38.802*.
[29] Efectele negative ale câmpului electromagnetic asupra sănătăţii. Preluat de pe electricalc.ro:
https://electricalc.ro/index.php?option=com_content&view=article&id=88&Itemid=319
[30] Câmpuri electromagnetice şi sănătatea publică: telefoane mobile. Preluat de pe: Electromagnetic fields and public health: mobile phones (who.int).
[31] Spectrul de frecvenţe radio. Preluat de pe: https://www.ancom.ro/spectru-radio_2749
[32] Morega M. (1999). Bioelectromagnetism. Ed. Matrix Rom, Bucuresti, ISBN 973-685- 056-0.
[33] Kraus, J. D., & Fleisch, D. A. (1999). *Electromagnetics: With Applications*. WCB/McGraw-Hill.
[34] Hasgall, P. A., Di Gennaro F., Baumgartner C., Neufeld E., Lloyd B., Gosselin M.C., Payne D., Klingenböck A., & Kuster N. (2022). "IT'IS Database for thermal and electromagnetic parameters of biological tissues," Version 4.1. Disponibil: itis.swiss/database
[35] Gorur G. R. (2003). Dielectrics in electric fields, Marcel Dekker Inc.
[36] Furse, C., Christensen, D.A., & Durney, C.H. (2009). Basic Introduction to Bioelectromagnetics (2nd ed.). CRC Press, p. 95.
[37] IEEE Standard for Safety Levels with Respect to Human Exposure to Radio Frequency Electromagnetic Fields, 3 kHz to 300 GHz. (2006). *IEEE Std C95.1-2005 (Revision of IEEE Std C95.1-1991)*, 1–238.
[38] Durney, C H, Massoudi, H, & Iskander, M F. *Radiofrequency radiation dosimetry handbook. 4th edition. Final report, 1 July 1984-31 December 1985*. United States.
[39] Frei, M. R. (1995). Frequency and Orientation Effects on Sites of Energy Deposition. În B. J. Klauenberg, M. Grandolfo, & D. N. Erwin (Ed.), *Radiofrequency Radiation Standards:*

Biological Effects, Dosimetry, Epidemiology, and Public Health Policy (pp. 295–301). Springer US.
[40] Chou, C. K., Bassen, H., Osepchuk, J., Balzano, Q., Petersen, R., Meltz, M., Cleveland, R., Lin, J. C., & Heynick, L. (1996). Radio frequency electromagnetic exposure: tutorial review on experimental dosimetry. *Bioelectromagnetics*, *17*(3), 195–208.
[41] Institute of Electrical and Electronics Engineers. (2005). *IEEE recommended practice for measurements and computations of radio frequency electromagnetic fields with respect to human exposure to such fields, 100 kHz-300 GHz* (IEEE Standard C95.3-2005). IEEE.
[42] The National Toxicology Program animal study. Preluat de pe: https://www.arpansa.gov.au/sites/default/files/advice_from_arpansa_on_ntp_study.pdf
[43] Michaelson, S. M. (1967). Effects of electromagnetic radiations on physiologic responses. *Aerospace Medicine, 38*, 293.
[44] INTERPHONE Study Group (2010). Brain tumour risk in relation to mobile telephone use: results of the INTERPHONE international case-control study. *International journal of epidemiology*, *39*(3), 675–694.
[45] Aydin, D., Feychting, M., Schüz, J., Andersen, T. V., Poulsen, A. H., Prochazka, M., Klæboe, L., Kuehni, C. E., Tynes, T., & Röösli, M. (2011). Predictors and overestimation of recalled mobile phone use among children and adolescents. *Progress in biophysics and molecular biology*, *107*(3), 356–361.
[46] Aydin, D., Feychting, M., Schüz, J., Röösli, M., & CEFALO study team (2012). Childhood brain tumours and use of mobile phones: comparison of a case-control study with incidence data. *Environmental health : a global access science source*, *11*, 35.
[47] Danker-Hopfe, H., Dorn, H., Bornkessel, C., & Sauter, C. (2010). Do mobile phone base stations affect sleep of residents? Results from an experimental double-blind sham-controlled field study. *American journal of human biology : the official journal of the Human Biology Council*, *22*(5), 613–618.
[48] Divan, H. A., Kheifets, L., & Olsen, J. (2011). Prenatal cell phone use and developmental milestone delays among infants. *Scandinavian journal of work, environment & health*, *37*(4), 341–348.
[49] Lăzărescu, C. (2012). *Interacţiunea câmpului electromagnetic cu materia vie*. Iaşi.
[50] Mat, M. H., Fareq Bin Abd Malek, M., Whittow, W. G., Ronald, S. R., & Zulkefl, M. S. (2013) The influence of human head model wearing metal-frame spectacles to the changes of sar and antenna gain: simulation of frontal face exposure. *Progress In Electromagnetics Research*, *137*, 453–473.
[51] Morimoto, R., Laakso, I., De Santis, V., & Hirata, A. (2016). Relationship between peak spatial-averaged specific absorption rate and peak temperature elevation in human head in frequency range of 1-30 GHz. *Physics in medicine and biology*, *61*(14), 5406–5425.
[52] Sasaki, K., Mizuno, M., Wake, K., & Watanabe, S. (2017). Monte Carlo simulations of skin exposure to electromagnetic field from 10 GHz to 1 THz. *Physics in medicine and biology*, *62*(17), 6993–7010.
[53] Mydlová, J., Beňová, M., Stefancova, V., & Pitlova, E. (2019). Assessment of SAR in human body model with the cochlear implant inside a railway vehicle. *TRANSCOM 2019 13th International Scientific Conference on Sustainable, Modern and Safe Transport*, *40*, 1489–1496.
[54] Christ, A., Samaras, T., Neufeld, E., & Kuster, N. (2020). RF-induced temperature increase in a stratified model of the skin for plane-wave exposure at 6-100 GHz. *Radiation protection dosimetry*, *188*(3), 350–360.
[55] Ramachandran, T., Faruque, M. R. I., & Islam, M. T. (2022). Specific absorption rate reduction for sub-6 frequency range using polarization dependent metamaterial with high effective medium ratio. *Scientific Reports*, *12*(1), 1803.

[56] Chiaraviglio, L., Bartoletti, S., Blefari-Melazzi, N., Lodovisi, C., Moretti, A., Zampognaro, F., & Alouini, M.-S. (2023). Measuring EMF and Throughput Before and After 5G Service Activation in a Residential Area. *IEEE Open Journal of the Communications Society*, *4*, 1179–1195.
[57] Jovanovic, D. B., Krasic, D., Cvetkovic, N. N., Vuckovic, D., & Stanković, V. B. (2023). Electric field and SAR distribution in the vicinity of dental implants exposed to the cell phone electromagnetic radiation. *COMPEL - The international journal for computation and mathematics in electrical and electronic engineering*, *42*(5), 1052–1067.
[58] Chiaraviglio, L., Lodovisi, C., Bartoletti, S., Elzanaty, A., & Slim-Alouini, M. (2024). Dominance of Smartphone Exposure in 5G Mobile Networks. *IEEE Transactions on Mobile Computing*, *23*(3), 2284–2302.
[59] Sadiku, M. N. O. (2000). *Numerical techniques in electromagnetics* (2nd ed.). Boca Raton, FL: CRC Press LLC.
[60] American Standards Association. (1996) Safety levels of electromagnetic radiation with respect to personnel, USASI standard C95.1.
[61] International Commission on Non-Ionizing Radiation Protection (ICNIRP). (1998). Guidelines for limiting exposure to time-varying electric, magnetic and electromagnetic fields (up to 300GHz), Health Physics, 74(4), pp. 494–522.
[62] Foster, K. R. (1908) Exposure Limits for Radiofrequency Energy: Three Models. University of Pennsylvania.
[63] International Commission on Non-Ionizing Radiation Protection (ICNIRP). (2020). Guidelines for limiting exposure to time-varying electric, magnetic and electromagnetic fields (up to 300GHz), Health Physics, 118(5), pp. 483–524.
[64] Adair, E. R., Adams, B. W., & Akel, G. M. (1984). Minimal changes in hypothalamic temperature accompany microwave-induced alteration of thermoregulatory behavior. *Bioelectromagnetics*, *5*(1), 13–30.
[65] Michaelson, S. M., & Elson, E. C. (1996) Modulated fields and 'window' effects. In: Polk, C.; Postow, E., eds. Biological effects of electromagnetic fields. Boca Raton, FL: CRC Press; pp. 435–533.
[66] Arens, E, & Zhang H. (2006). Skin's role in human thermoregulation and comfort. In: Pann N, Gibson P, eds. Thermal and moisture transport in fibrous materials. Cambridge, England: Woodhead Publishing Ltd, pp. 560–602.
[67] Shafahi, M., & Vafai, K. (2010). Human Eye Response to Thermal Disturbances. *Journal of Heat Transfer*, *133*(011009).
[68] Foster, K. R., Ziskin, M. C., & Balzano, Q. (2016). Thermal Response of Human Skin to Microwave Energy: A Critical Review. *Health physics*, *111*(6), pp. 528–541.
[69] Kodera, S., Hirata, A., Funahashi, D., Watanabe, S., Jokela, K., & Croft, R. J. (2018). Temperature Rise for Brief Radio-Frequency Exposure Below 6 GHz. *IEEE Access*, *6*, 65737–65746.
[70] IEEE Standard for Safety Levels with Respect to Human Exposure to Electric, Magnetic, and Electromagnetic Fields, 0 Hz to 300 GHz. (2019). *IEEE Std C95.1-2019 (Revision of IEEE Std C95.1-2005/ Incorporates IEEE Std C95.1-2019/Cor 1-2019)*, 1–312.
[71] Torres, V. B., Christ, A., & Kuster, N. (2006). *SAR Distribution in Test Animals Exposed to RF Radiation*.
[72] Panagopoulos, D. J., Johansson, O., & Carlo, G. L. (2013). Evaluation of specific absorption rate as a dosimetric quantity for electromagnetic fields bioeffects. *PloS one*, *8*(6), e62663.
[73] Miclăuş S. (2007). Dozimetria câmpurilor electromagnetice de radiofrecvenţă şi microunde – elemente teoretice şi experimentale. Ed. Academiei Forţelor Terestre, Sibiu.
[74] CST Microwave Studio. Preluat de pe: www.cst.com.

[75] Weiland, T. (1977). A discretization method for the solution of Maxwell's equations for sixcomponent fields: Electronics and Communication, (AEÜ), vol. 31, pp. 116-120.
[76] Clemens, M., & Weiland, T. (2001). Discrete Electromagnetics: Maxwell's Equations Tailored to Numerical Simulations. ICS Newsletter, vol. 8 (2).
[77] Weiland, T. (1996). Time Domain Electromagnetic Field Computation with Finite Difference Methods. *International Journal of Numerical Modelling*, vol. 9, pp. 295-319.
[78] Krietenstein, B., Thoma, P., Weiland, T., & Schuhmann, R. (1998). *The Perfect Boundary Approximation Technique Facing the Big Challenge of High Precision Field Computation*, pp. 860-862.
[79] Electromagnetic Simulation Solvers. Preluat de pe 3ds.com: https://www.3ds.com/products/simulia/cst-studio-suite/electromagnetic-simulation-solvers
[80] National Observatory of Electromagnetic Fields. Preluat de pe: https://paratiritirioemf.eeae.gr/en/.
[81] Apostolidis, C., Manassas, A., Iakovidis, S., & Samaras, T. (2022). Electromagnetic Fields in the Environment: An Update of Monitoring Networks in Europe. *2022 3rd URSI Atlantic and Asia Pacific Radio Science Meeting (AT-AP-RASC)*, 1–3.
[82] Djuric, N., Skoric, T., Kljajic, D., Otasevic, V., & Djuric, S. (2023). A Hidden Knowledge in Long-Term EMF Monitoring of EMF RATEL Monitoring Network. *2023 Photonics & Electromagnetics Research Symposium (PIERS)*, 1856–1861.
[83] Hartă privind monitorizarea câmpului electromagnetic. Preluat de pe: https://www.monitor-emf.ro/.
[84] Kurnaz, C., & Mutlu, M. (2020). Comprehensive radiofrequency electromagnetic field measurements and assessments: A city center example. *Environmental Monitoring and Assessment*, *192*(6), 334.
[85] Ursachianu, M., Bejenaru, O., Lazarescu, C., Salceanu, A., & Paulet, M. (2021). The Assessment of Human Exposure in Iasi-City using Data Provided by The National Autonomous RF-EMF Monitoring System throughout 2020. *2021 International Conference on Electromechanical and Energy Systems (SIELMEN)*, 225–230.
[86] Lopes, M. A., Zhang, J., Krzemiński, D., Hamandi, K., Chen, Q., Livi, L., & Masuda, N. (2021). Recurrence quantification analysis of dynamic brain networks. *The European journal of neuroscience*, *53*(4), 1040–1059.
[87] Eckmann, J.-P., Kamphorst, S. O., & Ruelle, D. (1987). Recurrence Plots of Dynamical Systems. *Europhysics Letters*, *4*(9), 973.
[88] Marwan, N., Carmen Romano, M., Thiel, M., & Kurths, J. (2007). Recurrence plots for the analysis of complex systems. *Physics Reports*, *438*(5), 237–329
[89] Guo, R., Wang, Y., Yan, J., & Yan, H. (2012). Recurrence quantification analysis on pulse morphological changes in patients with coronary heart disease. *Journal of traditional Chinese medicine*, *32*(4), 571–577.
[90] Melillo, P., Bracale, M., & Pecchia, L. (2011). Nonlinear Heart Rate Variability features for real-life stress detection. Case study: students under stress due to university examination. *Biomedical engineering online*, *10*, 96.
[91] Eckmann, J.-P., Kamphorst, S. O., & Ruelle, D. (1987). Recurrence Plots of Dynamical Systems. *Europhysics Letters*, *4*(9), 973.
[92] Webber, C. L., & Zbilut, J. P. (2007). Recurrence quantifications: feature extractions from recurrence plots. *International Journal of Bifurcation and Chaos*, *17*(10), 3467–3475.
[93]Aaronia Spectran V5 X. (10.06.2023). Preluat de pe aaronia.com: https://downloads.aaronia.com/datasheets/analyzers/V5/V5-X.pdf

[94] Near-Field Probes. (10.06.2023). Preluat de pe aaronia.com: https://aaronia.com/antennas/rf-and-near-field-probes/
[95] R&S TSMA6 user manual. (10.06.2023). Preluat de pe rohde-scwarz.com: https://www.rohde-schwarz.com/nl/manual/r-s-tsma6-user-manual-manuals_78701-572421.html
[96] OmniLOG antenna. (10.06.2023). Preluat de pe aaronia.com: https://tele-grup.ro/wp-content/uploads/2016/09/Specificcatii-Tehnice-OmniLOG-90200.pdf
[97] Miclaus, S., Deaconescu, D. B., Vatamanu, D., & Buda, A. M. (2022). The temporal imprint of mobile phone emission level when running various applications in 4G versus 5G networks. *2022 International Symposium on Electronics and Telecommunications (ISETC)*, 1–4.
[98] Deaconescu, D. B., Maria Buda, A., Suka, D., & Miclaus, S. (2023). Temporal Recurrence Analysis of Base Stations Emissions in 4G Mobile Communications. *2023 13th International Symposium on Advanced Topics in Electrical Engineering (ATEE)*, 1–8.
[99] Takens, F. (1981). Detecting strange attractors in turbulence. În D. Rand & L.-S. Young (Ed.), *Dynamical Systems and Turbulence, Warwick 1980* (pp. 366–381). Springer Berlin Heidelberg.
[100] Fraser, A. M., & Swinney, H. L. (1986). Independent coordinates for strange attractors from mutual information. *Phys. Rev. A*, *33*(2), 1134–1140.
[101] Kennel, M. B., Brown, R., & Abarbanel, H. D. I. (1992). Determining embedding dimension for phase-space reconstruction using a geometrical construction. *Phys. Rev. A*, *45*(6), 3403–3411.
[102] Fabretti, A., & Ausloos, M. (2005). Recurrence plot and recurrence quantification analysis techniques for detecting a critical regime. *International Journal of Modern Physics C*, *16*(05), 671–706.
[103] Nayak, S. K., Bit, A., Dey, A., Mohapatra, B., & Pal, K. (2018). A Review on the Nonlinear Dynamical System Analysis of Electrocardiogram Signal. *Journal of healthcare engineering*, *2018*, 6920420.
[104] Colombelli, A, & Tunzelmann, N. (2011). The persistence of innovation and path dependence. Handbook on the Economic Complexity of Technological Change, Edward Elgar Publishing Limited, Cheltenham, UK, pp. 105–119.
[105] Webber, C. L., Jr, & Zbilut, J. P. (1994). Dynamical assessment of physiological systems and states using recurrence plot strategies. *Journal of applied physiology (Bethesda, Md. : 1985)*, *76*(2), 965–973.
[107] Kraemer, K. H., Donner, R. V., Heitzig, J., & Marwan, N. (2018). Recurrence threshold selection for obtaining robust recurrence characteristics in different embedding dimensions. *Chaos (Woodbury, N.Y.)*, *28*(8), 085720.
[107] Ye, H., Deyle, E. R., Gilarranz, L. J., & Sugihara, G. (2015). Distinguishing time-delayed causal interactions using convergent cross mapping. *Scientific Reports*, *5*(1), 14750.
[108] Dangi, R., Lalwani, P., Choudhary, G., You, I., & Pau, G. (2021). Study and Investigation on 5G Technology: A Systematic Review. *Sensors (Basel, Switzerland)*, *22*(1), 26.
[109] Bonato, M., Dossi, L., Gallucci, S., Benini, M., Tognola, G., & Parazzini, M. (2022). Assessment of Human Exposure Levels Due to Mobile Phone Antennas in 5G Networks. *International journal of environmental research and public health*, *19*(3), 1546.
[110] Joshi, P., Ghasemifard, F., Colombi, D., & Törnevik, C. (2020). Actual Output Power Levels of User Equipment in 5G Commercial Networks and Implications on Realistic RF EMF Exposure Assessment. *IEEE Access*, *8*, 204068–204075.
[111] Lee, A.-K., Jeon, S.-B., & Choi, H.-D. (2021). EMF Levels in 5G New Radio Environment in Seoul, Korea. *IEEE Access*, *9*, 19716–19722.

[112] Miclaus, S., Deaconescu, D.-B., Vatamanu, D., Buda, A. M., Sarbu, A., & Pindaru, B. (2022). Peculiarities of the radiated field in the vicinity of a mobile terminal connected to 4G versus 5G networks during various applications usage. *AIMS Electronics and Electrical Engineering*, *6*(2), 161–177.
[113] Deaconescu, D. B., Buda, A. M., Vatamanu, D., & Miclaus, S. (2022). The Dynamics of the Radiated Field Near a Mobile Phone Connected to a 4G or 5G Network. *Engineering, Technology & Applied Science Research*, *12*(1), 8101–8106.
[114] Gultekin, D. H., & Siegel, P. H. (2020). Absorption of 5G Radiation in Brain Tissue as a Function of Frequency, Power and Time. *IEEE Access*, *8*, 115593–115612.
[115] Hardell, L., & Nilsson, M. (2023). The Microwave Syndrome after Installation of 5G Emphasizes the Need for Protection from Radiofrequency Radiation. *Case Report*, vol. 8, 1112.
[116] Ayad, M., Alkanhel, R., Saoudi, K., Benziane, M., Medjedoub, S., & Ghoneim, S. S. M. (2022). Evaluation of Radio Communication Links of 4G Systems. *Sensors*, *22*(10).
[117] Imam-Fulani, Y. O., Faruk, N., Sowande, O. A., Abdulkarim, A., Alozie, E., Usman, A. D., Adewole, K. S., Oloyede, A. A., Chiroma, H., Garba, S., Imoize, A. L., Baba, B. A., Musa, A., Adediran, Y. A., & Taura, L. S. (2023). 5G Frequency Standardization, Technologies, Channel Models, and Network Deployment: Advances, Challenges, and Future Directions. *Sustainability*, *15*(6).
[118] Miclaus, S., & Bechet, P. (2020). Non-stationary statistics with Amplitude Probability Density Function for exposure and energy density reporting near a mobile phone running 4G applications. *Progress In Electromagnetics Research M,* vol. 89, pp. 151–159.
[119] Sârbu, A., Bechet, A., Bălan, T., Robu, D., Bechet, P., & Miclăuş, S. (2019). Using CCDF statistics for characterizing the radiated power dynamics in the near field of a mobile phone operating in 3G+ and 4G+ communication standards. *Measurement*, *134*, 874–887.
[120] Zou, Z., Shi, Z., Guo, Y., & Ye, J. (2019). Object detection in 20 years: A survey. *IEEE Transactions on Pattern Analysis and Machine Intelligence, 43*(3), 821-836.
[121] Li, J., & Zhao, Z. (2022). YOLOv7: A new state-of-the-art object detection model. *Technical Report*.
[122] R&S®FSV3000 Signal and spectrum analyzer. (05.03.2023). Preluat de pe rohde-schwarz.com: https://www.rohde-schwarz.com/us/products/test-and-measurement/benchtop-analyzers/rs-fsv3000-signal-and-spectrum-analyzer_63493-601503.html
[123] R&S®FSW26 Signal and spectrum analyzer. (05.03.2023). Preluat de pe rohde-schwarz.com: https://www.rohde-schwarz.com/us/products/test-and-measurement/benchtop-analyzers/fsw-signal-and-spectrum-analyzer_63493-11793.html
[124] OmniLOG antenna. (05.03.2023). Preluat de pe aaronia.com https://aaronia.com/en/ultra-broadband-antenna-omnilog-30800
[125] Wang, C.-Y., Yeh, I.-H., & Liao, H.-Y. M. (2024). *YOLOv9: Learning What You Want to Learn Using Programmable Gradient Information* (arXiv:2402.13616).
[126] Lavanya, G., & Pande, S. D. (2023). Enhancing Real-time Object Detection with YOLO Algorithm. *EAI Endorsed Transactions on Internet of Things*, *10*.
[127] Shaw, J.W. (2013). Radiometry and the Friis transmission equation. *American Journal of Physics*, vol. 81, pp. 33–37.
[128] Miclaus, S., Deaconescu, D. B., Vatamanu, D., & Buda, A. M. (2023). An Exposimetric Electromagnetic Comparison of Mobile Phone Emissions: 5G versus 4G Signals Analyses by Means of Statistics and Convolutional Neural Networks Classification. *Technologies*, *11*(5).
[129] Ojaroudi Parchin, N., Jahanbakhsh Basherlou, H., & Abd-Alhameed, R. A. (2020). Design of Multi-Mode Antenna Array for Use in Next-Generation Mobile Handsets. *Sensors*, *20*(9).

[130] Betta, G., Capriglione, D., Cerro, G., Miele, G., Migliore, M. D., & Šuka, D. (2022). Experimental analysis of 5G pilot signals' variability in urban scenarios. *2022 IEEE International Symposium on Measurements & Networking (M&N)*, 1–6.
[131] Betta, G., Capriglione, D., Cerro, G., Miele, G., Migliore, M. D., & Šuka, D. (2022). 5G DSS communications: Pilot signals' variability analysis from measurements on the field. *2022 IEEE International Instrumentation and Measurement Technology Conference (I2MTC)*, 1–6.
[132] Chiaraviglio, L., Turco, S., Bianchi, G., & Blefari-Melazzi, N. (2022). "Cellular Network Densification Increases Radio-Frequency Pollution": True or False? *IEEE Transactions on Wireless Communications*, *21*(4), 2608–2622.
[133] Bonato, M., Dossi, L., Chiaramello, E., Fiocchi, S., Tognola, G., & Parazzini, M. (2021). Stochastic Dosimetry Assessment of the Human RF-EMF Exposure to 3D Beamforming Antennas in indoor 5G Networks. *Applied Sciences*, *11*(4).
[134] Rashid, M., & Hossain, S. (2014). Antenna solution for millimeter wave mobile communication (MWMC): 5G. *International Journal of Scientific & Technology Research*, vol. 3, pp. 1157-1161.
[135] Bodwin, G. T., Chung, H. S., & Repond, J. (2019). Implementation of Maxwell's equations in the reconstruction of the magnetic field in the g−2 storage ring. *Journal of Instrumentation*, *14*(07), P07002.
[136] Deaconescu, D. B., & Miclaus, S. (2023). The 5G-FR1 Signals: Beams of the Phased Antennas Array and Time-Recurrence of Emissions with Consequences on Human Exposure. *Electronics*, *12*(2).
[137] Tissue dielectric properties of body tissues. Preluat de pe niremf.ifac: http://niremf.ifac.cnr.it/tissprop/htmlclie/htmlclie.php
[138] Wu, T., Rappaport, T. S., & Collins, C. M. (2015). Safe for Generations to Come. *IEEE microwave magazine*, *16*(2), 65–84.